ELECTROACTIVE SELF-HEALING SOFT ROBOTIC GRIPPER

Master Thesis Project

ABSTRACT

Soft robots are good candidates for replacing rigid metallic robots due to their flexible properties and ease to comply with different environments. A drawback that comes with their soft characteristics is their susceptibility to damage over repeated actuations. In this work, we developed a soft robotic actuator with self-healing capabilities. Unlike most of the studied soft robots actuated by pneumatic pressure, the robot developed in this work bends due to phase transition of the liquid contained inside. The pressure required to achieve bending actuation is generated by the electrically induced phase transition of ethanol at elevated temperatures. Carbon black is added together with ethanol to improve heat distribution and actuation time. The self-healing effect can be induced by the same electrical stimulus in the same temperature range necessary to achieve motion. Critical parameters such as the mass of liquid, carbon black and voltage were optimized in order to maximize actuation speed. The actuator can achieve bending in less than 1 minute at power inputs lower than 30 W.

Diana-Patricia Horvat

1st supervisor: Ranjita K. Bose

2nd supervisor: Francesco Picchioni

Daily supervisor: Felipe Orozco Gutierrez

Table of Contents

1. Introduction

Robotics is a ubiquitous field that is rising rapidly in today's society. The most well studied and currently implemented are industrial robots designed to perform improved human- or animal-like tasks with increased strength, speed and precision. Physical compatibility between robots and humans could extend the range of applications, making robots suitable to operate in more elaborate contexts such as the medical field, for example, as prosthetics or artificial muscles. Existing hard robots present limitations when it comes to achieving biocompatibility due to the rigid materials they are made of. Additionally, given their in-built motors and solenoids, hard robots tend to be inefficient when it comes to their energy use and are rather heavy. They require precise positioning in order to carry out tasks, as they are not designed to change their shape in order to adapt to new environments or functions. This makes them unsuitable to operate safely in close proximity to fragile objects or humans. In other words, they can perform complex motions with good precision, while suffering from the non-compliant behavior of the materials they are built with and the complexity of the systems they are operated by.[1,2]

Soft robotics have risen due to the need for safe interactions between robots and people. Soft materials can be characterized as particularly soft, flexible and easy to deform, such as elastomeric polymers that include silicones and polyurethanes.[3] This type of materials have a modulus that is compliant with biological tissues and organs, which makes them good candidates for applications that mimic environmental interactions. As opposed to hard robots, soft materials can readjust their shape when in contact with different objects, giving them the ability to function safely in close contact with people or as grippers that handle delicate objects (e.g.: fruits, vegetables). Generally soft robots can be actuated with a simple sensor or external stimulus, such as pressure or electricity, which makes them lightweight and easy to handle.[4–6] Their commercial availability is already in place from companies like Soft Robotics Inc. and Empire Robotics with a focused application in agriculture, packaging and picking of irregular objects.

Several factors affect the properties, functionality, shelf life and actuation of commercial soft robots, including their formation materials, modes of actuation and self-healing abilities. In the upcoming sections, these factors are discussed in order to assess how they individually influence the final properties of the soft robots.

1.1. Materials

To identify the contribution of the different materials that have been used to develop soft robots and how the properties of these elements engender distinct properties in the final robot, an overview of the typical materials used in the manufacturing of soft robotics will be discusses in this section.

Soft robots are typically designed using silicone elastomers, urethanes and hydrogels.[7] Due to their extended range of elastic and viscoelastic properties, elastomers are popular candidates for this field. They interact safely with biological organisms, including humans, and have a decreased stiffness when compared to rigid robots constructed from metals or hard plastics. [8] While the latter are characterized by an elastic modulus between 10^9 - 10^{12} Pa, tissues, skin or cartilages have moduli in the range of 10^2 - 10^9 Pa.[9] Given that the elastomers used in the manufacturing of soft robots have moduli that overlap the range present in natural organisms, they have the capability to adapt their shape when a force is applied by means of elastic deformation. This mechano-compatibility allows a reduction in the impact stress and a better contact time over a wider area. Some examples of silicone elastomers that are compliant with the characteristics described are Sylgard 184 polydimethylsiloxane (PDMS) from Dow Chemicals, Smooth-Sil 950 and Ecoflex from Smooth-On.[10] As an example, Ecoflex is a silicone-based elastomeric polymer with a modulus between 10^5 - 10^6 Pa.

Considering that viscoelasticity is a popular trait among soft robotic materials, their performance can be assigned in terms of their storage and loss modulus (their elastic and viscous part, respectively). Some examples of purely elastic materials are bone, wood, steel and they are characterized by a lack of energy dissipation when under load, which translates into very low loss modulus. In contrast, viscoelastic materials such as tissues, muscle, PDMS, hydrogels, etc. show a combination of elastic and viscous responses (viscoelasticity), which allows them to accommodate their properties under load due to energy dissipation, while remaining steady in their trajectory. A summary of different materials with potential applications in soft robotics based on their storage vs loss modulus is represented in *Figure 1*.[8]

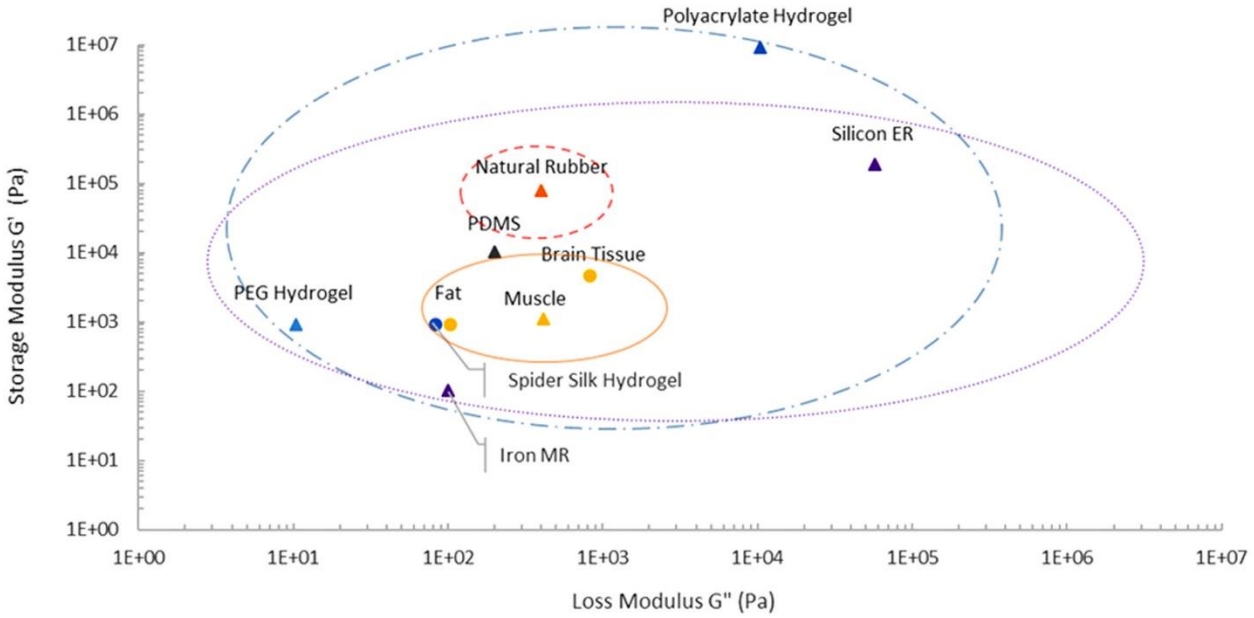

Figure 1. *Representation of the storage vs loss modulus for different materials with potential applications in soft robotics; hydrogels are crossed by a blue discontinuous line; biological tissues are crossed by a yellow continuous line and natural rubbers are crossed by an orange discontinuous line; triangles represent materials that were previously utilized in soft robots. Figure taken from* [8]

Depending on the application requirements, the material selection is important to be considered in terms of several different properties. Certain viscoelastic materials exhibit elastic hysteresis, such as polyacrylates and urethanes.[11] Silicones are used for applications that require increased cycle loading or elastic resilience.[12] Certain types of hydrogels, such as double networks with either ionic or covalent crosslinks exhibit high fracture toughness.[13] Work energy density describes the volumetric capacity of a device required in order to attain a specific work and is inversely proportional to the volume, as depicted in *Equation 1*. *Figure 2* summarizes specific energy densities of different types of materials as a function of the Young's modulus. There is a trade-off between material compliance and stiffness or energy density, as the higher the energy density is, the higher the stiffness and the less compliant the material becomes.[8]

$$U = \frac{E}{V} \qquad (1),$$

where:

U= Work energy density $[J/m^3]$

E= Energy stored [J]

V= Volume $[m^3]$

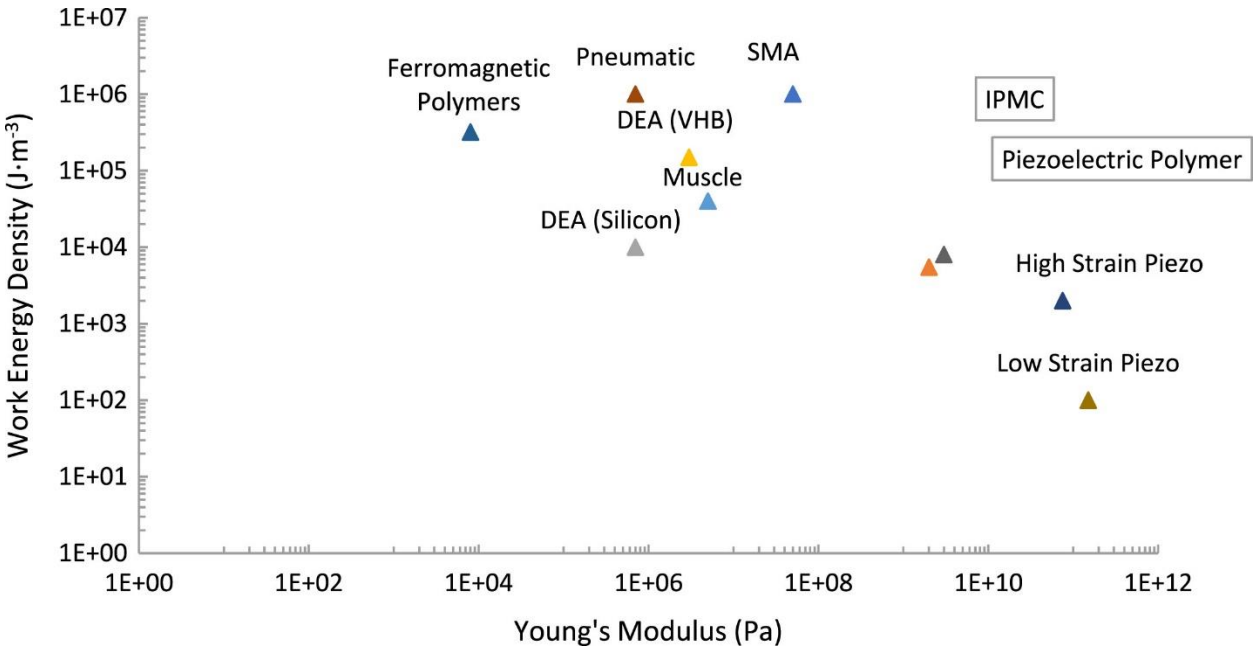

Figure 2. *Representation of work density vs Young's modulus for different types of materials; DEA=dielectric elastomers; SMA=shape memory alloys, IPMC=ionic polymer-metal composite. Figure taken from* [8]

Another class of materials with potential in the manufacturing of soft robots are shape memory polymers. Shape memory polymers (SMPs) are smart materials characterized by their ability to display mechanical action as a result of an external stimulus application. SMPs consist of a stable network that retains the original shape and at least one reversible switching phase. The former can be implemented by means of chemical crosslinking, crystalline phase, interpenetrated networks or molecule entanglement. The switching phase is temporarily fixed through reversible covalent or noncovalent bonds (e.g. Diels-Alder reactions, supramolecular interactions), crystallization (temperatures above T_m would result in the recovery of the original shape), a glass transition, different liquid crystalline phase transitions, etc, and can be summarized in *Figure 2.* [14]

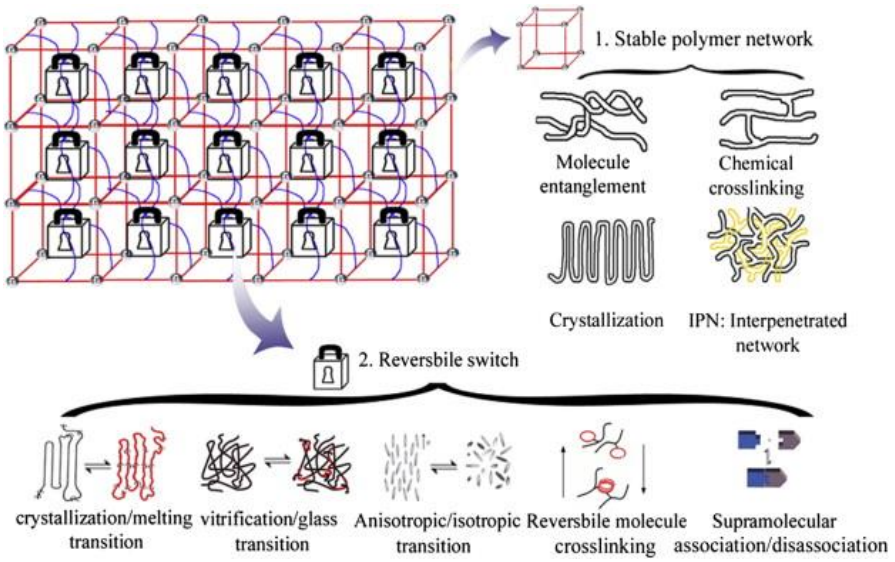

Figure 3. *Schematic representation of the two phases contained in an SMP: the stable network and the switching phase. The stable network can be achieved by molecule entanglement, crystallization, chemical crosslinking and interpenetrated network, while the reversible phase can be achieved by crystallization/melting transition, vitrification/glass transition, transition between different crystalline structures, reversible molecule crosslinking and supramolecular association/dissociation. Figure taken from* [15]

As the soft robotics technology is evolving, so are the types of materials used and the methods of construction. A common procedure of fabrication is drop-casting of the material into molds. However, recent technological advances make 3D printing of the actuators possible, conferring cost-effectiveness when it comes to mass production of soft robots. The drawback in this approach is that the tensile strength of the material is decreased, which results in higher breaking ease when compared to other soft robotic actuators. Research in this field suggests that the tensile strength of 3D printed materials can be improved.[1]

1.2. Modes of actuation

Actuators are defined as devices that provide energy to another device by means of motion or mechanical work. An overview of the typical actuation mechanisms that are being explored in the manufacturing of devices triggered by different stimuli are examined in this section with recent examples from literature with an assessment and comparison of their performance.

Typical examples of devices used as actuators are pneumatic pistons and electric motors. Machines can be defined as mechanical systems composed of different parts utilized to execute different tasks. Robots, on the other hand, consist of machines that are meant to mimic tasks performed by humans or animals' motions, an example being grippers.[2]

Considering that the main focus of this thesis is to develop a gripper, different approaches were considered and investigated. Firstly, motion could be induced by programming the self-healing material chosen in this work into a certain shape and actuating it to (un)bend upon stimulus, considering that it has shape memory properties. Secondly, bilayer actuators composed of materials that behave differently upon stimulus impulse could result in a bending motion. Lastly, soft robotic actuators with more complex geometries and design could attain gripping applications with different stimuli. Although bi-layer actuators (2D) could be included in the soft robotic actuator category, for better clarity upon the wide range of different studies reported, this work will consider soft robots as materials that contain more complex (mainly 3D) geometries. All the different modes of actuation are introduced below, starting with a brief description on what shape memory polymers entail, to more in-depth literature research on the up-to-date reports in the field on different bilayer actuators and soft robotic grippers.

1.2.1. Shape memory polymers

The most common triggers used in the actuation of SMPs are heat or light, although magnetic, electric, pH and other triggers can be used. In order to obtain the fixed shape, the permanent shape above the 'switch temperature' T_{SW} must be first processed, generally done by extrusion, spinning or pressing, followed by the programming of the temporary shape. The latter is obtained by controlled mechanical action applied to the material at temperatures above or below T_{SW}. When the material is exposed to temperatures that beyond T_{SW}, this will return to its permanent shape - a cycle that can be repeated multiple times. The two most commonly used transitions in the actuation of the shape memory effect (SME) are the thermal ones, namely the melting (T_m) and the glass transition (T_g) temperatures. The first one corresponds to materials such as rubbers that are chemically crosslinked, semicrystalline polymers and polymers that are physically crosslinked, while the second is utilized in thermosets that are chemically cross-linked and physically cross-linked thermoplastics. [14]

Although innovative, substantial improvements to the simple shape-memory effect (SME) described above are desired in order to suit certain applications. Given the non-reversibility of the shape change, also known as 'one way SME', the material requires reprogramming in order to attain the temporary shape again. A more desirable feature consists of the ability to reversibly switch between shapes without the need to reprogram the material in between cycles, a property known as a 'two-way SME'. Triple and multiple SMEs can be programmed, with two or more temporary shapes that can be triggered at different stimulus conditions, with the ability to return to the permanent shape. [16–18] Although in its infancy, the development of SMP actuators is a rising

field. A simple SMP was developed by fused-deposition modeling (FDM) 3D printing, where different parameters such as extruder temperature and scanning speed were investigated on their effect on the quality of the final product.[19] Two-way chemically cross-linked poly(ethylene-co-vinyl acetate) SMPs showing contraction with heating and expansion when cooled could find applications in artificial muscles.[20] Bodaghi et al. developed polyurethane-based dual and triple SMPs by means of hot-cold programming with biomedical applications. [21] The same FDM 3D printing technology was used, having as one of the potential applications a self-bending gripper.

1.2.2. Bilayer actuators

Bilayer actuators are another type of devices that, similarly to shape memory polymers, change their shape as a result of external stimuli, such as temperature, pH, light etc., and, as a result, exert mechanical work. Due to those properties, they find applications in medicine, robotics, microfabrication, etc. A classification of the different types of polymeric bilayer actuators up to date can be made, according to Ionov (2015)[22], as follows:

1.2.2.1. Bilayer actuators based on the elastic shape relaxation post-deformation

These types of actuators comprise, for example, the elastomers that operate based on electrical actuation when placed between two electrodes, also known as dielectric elastomer actuators (DEAs).[23] When the voltage is on, the electrodes attract each other resulting in the compression of the elastomer, which can later recover its shape when the voltage is off. A different example can be found in the shape recovery of elastomers with inhomogeneous cross-linking densities. [24] SMPs also work by a similar principle. As already mentioned in the previous section, the programming of SMPs is done by 'freezing' the temporary shape at a low temperature. As the temperature is increased, their flexibility is regained and they can return to their original shape. Although most SMPs are limited by their irreversibility, Behl et al. (2013) reported bi-layer SMP actuators with different switching temperatures, however this falls into the *1.2.2.3.* section.[25]

1.2.2.2. Bilayer actuators based on liquid-crystalline structures

Liquid-crystalline actuators work by having a reversible transition between an ordered and a disordered state. One example in this category is the fabrication of a dual-stimuli responsive bilayer actuator made of a light-triggered liquid crystal network (LCN) layer and an electricity-actuated polydimethylsiloxane (PDMS) composite layer.[26] Another study reported the design of

an LCN actuator engineered to function based on the selective decrosslinking of the polymer triggered optically.[27]

1.2.2.3. Bilayer actuators based on volume change

Two different types of actuations based on volume change can be considered. Firstly, hydrogels swell in water and shrink when dehydrated and can function in both aqueous conditions or high humidity. A second type of actuation is due to volume change with temperature, where thermal expansion or reduction occur at different temperature conditions. Melting and crystallization of polymers have a similar effect.[22] A self-healing glycerol-hydrogel with dual-response actuator that can be triggered by dry environments or increased temperatures was fabricated by Guo et al. (2019)[28]. Visible-light-responsive hydrogel-based actuators were designed with a self-healing effect.[29] Behl et al. (2013)[25] developed an actuator composed of two different SMPs with different melting temperatures, where the polymer with the higher T_m is responsible for the shape shifting and the one with the lower T_m gives the actuation. Reversibility is given by the change in volume upon transition from a melting/crystallization state of one of the layers. Hu et al. (2019)[30] designed a cellulose composite/PDMS bi-layer actuator that deforms bi-directionally under voltage and water absorption/desorption. A CNT/PDMS bi-layer actuator was developed that can be thermally triggered in one direction into the volume expansion of the PDMS layer.[31] Similarly, Wang et al. (2018)[32] developed a CNT-PDMS/GO bi-layer actuator that can be triggered by temperature, moisture and light irradiation. A simple two-layer silicone rubber-based actuator with thermal expansion microspheres that enlarge their volume at different temperatures was engineered, however the irreversibility of the expansion makes it unfavorable.[33] A PDMS/liquid crystal network (LCN) device was developed that was actuated by both magnetic and light irradiation. Both magnetic field and light triggering result in the thermal expansion of the LCN layer and an unbending effect of the originally bent bilayer.[26]

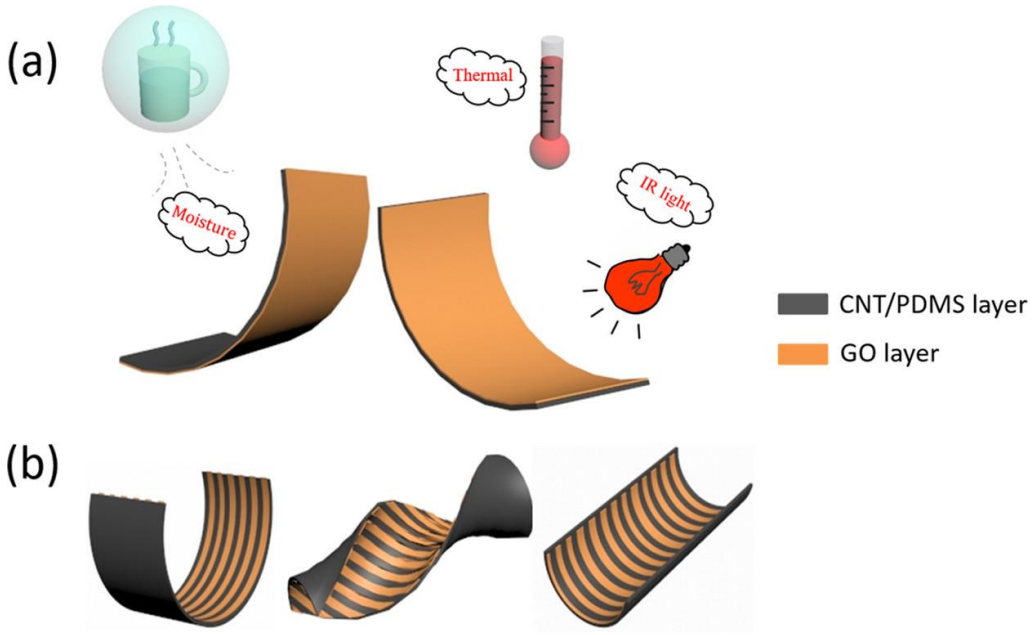

Figure 4. *Depiction of a bilayer actuator based on volume change a) triggered by moisture, temperature and IR light, b) with a bending deformation in different directions. Figure taken from* [32]

1.2.3. Soft robotic actuators

Further investigations were done on 3D soft robotics in order to expand the range of possible designs that could be adopted when manufacturing an actuator. Therefore, based on the review written by El-Atab et al. regarding the different actuation methods of soft robotic applications (but not limited to its content), a new classification can be summarized below. [34] It is worth noting that the classification was made on the basis of the external stimulus used to achieve motion within the soft robot, rather than the actual stimulus the actuator is driven by, which will be observed that in some cases is (indirect) pressure.

1.2.3.1. Thermally responsive actuators

Since the shape-memory effect plays an important role in the description of those types of materials, it can be observed that the actuation methods coincide with the ones mentioned when describing shape-memory polymers. Therefore, thermal radiation, Joule heating and light (visible, infrared, NIR) are a few direct and indirect heating methods that trigger the actuation. This type of actuation is safer in terms of handling when compared to voltage actuation, however, the actuation time can be rather slow.[34] Self-folding of 2D patterns into 3D geometries is of interest, with potential applications in drug delivery containers, reconfigurable devices, sensors,

etc.[35] Hinges composed out of SMPs are applied on 2D planes and upon (indirect) thermal stimulus they can make the plane bend and fold. Polyimide-based hinges, for example, show contraction when exceeding temperatures of 500 °C.[34] Thermally responsive soft robotic actuators based on volume change as a consequence of ethanol liquid-vapor phase transition entrapped in the device were reported. The material used for the matrix was a soft silicone-based polymer named $Ecoflex^{®}$. The device was made out of four layers, including a polymer nanofiber mat imbibed with ethanol that could provide a uniform dispersion of the liquid in order to achieve an even volume expansion and a paper layer that acted as the passive layer (with no volume expansion).[36]

1.2.3.2. Pneumatic actuators

Pneumatic actuators are an emerging technology designed by the Whitesides research group from Harvard University under the name of PneuNets.[37] Those are devices typically made out of a silicone-based soft materials, such as a Ecoflex, that achieve their actuation by applying pressure through a hollow tubing across the actuator. A multitude of shapes have been explored in the past decade, however, when it comes to grapplers, the series of hollow chambers contained inside an elastomer depicted in *Figure 5* has been the most studied shape. It is typically designed by having a more flexible type of silicone rubber used for the chambers, such as Ecoflex, while the side facing the object to be grabbed is made out of Sylgard 184. Both of the materials are PDMS based elastomers, with the difference that Ecoflex has a lower Young's modulus. Studies have been conducted on the optimization of the geometry in order to decrease the actuation time.[6] A more recent publication designed a PneuNet made out of a self-healing polymer that works by the reversible Diels-Alder principle, shown in *Figure 9.*[38] An Ecoflex/Cellulose device was fabricated where the cellulose layer was used as the passive layer, while the Ecoflex would expand as a result of pressure applied to the actuator, resulting in a bending motion.[39]

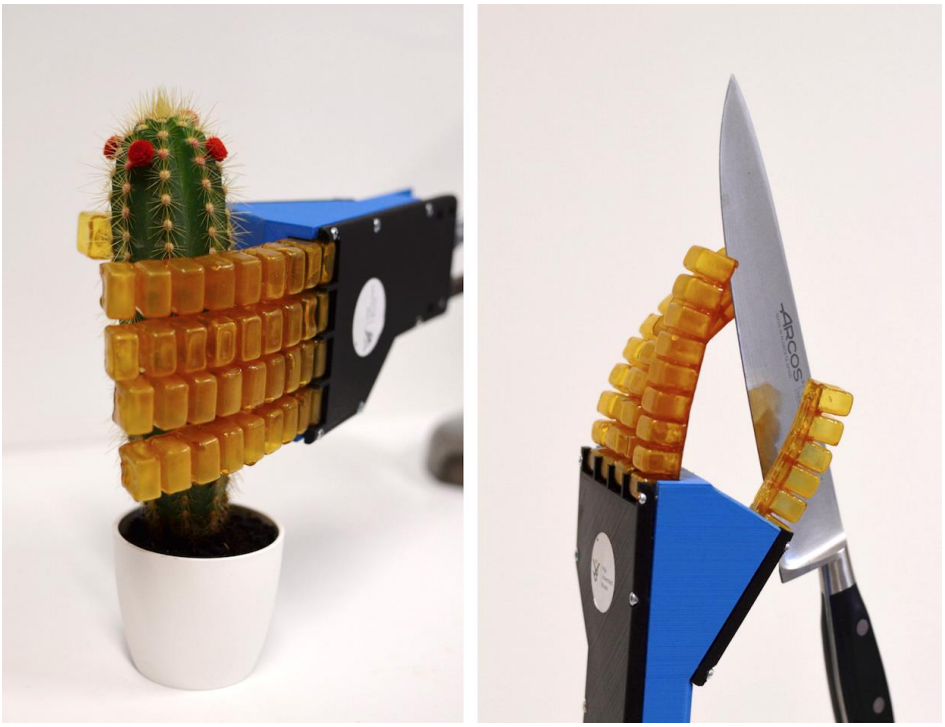

Figure 5. *Self-healable pneumatic actuators. Figure taken from* [38]

1.2.3.3. Electrically responsive actuators

In this category fall the flexible materials that can convert electrical energy into mechanical, such as liquid metals, some polymers, carbon-based materials etc. Typical applications for these types of materials are artificial muscles[40], microrobots[41], micrometer size manipulators[42], etc. Dielectric elastomer actuators (DEAs) represent a main class of materials that describe this type of actuation. DEAs are characterized by high flexibility, strain and energy density, while their performance is proportional to the voltage and the dielectric constant that characterizes the particular elastomer of use. Their drawbacks stand in the high voltage required for their applicability (in the range of kV) and the leakage currents.[43]

The most suitable DEAs in order to obtain effective actuations are acrylic elastomers, polyurethanes, silicones and rubbers. As opposed to acrylic elastomers, silicone-based and polyurethane elastomers show faster actuation with ease in tuning the shape and softness, however their strain is reduced in comparison. The silicone based elastomers permittivity is reduced in comparison to the other two types of elastomers mentioned, which results in the requirement of high activation voltage.[44] Research on the development of DEAs with higher dielectric constants by incorporating microparticles or the development of entirely organic elastomers has been carried out in recent years.[45] Although DEAs are characterized by high

actuation strain and efficiency, the high electric current required can result in failure. Liquid elastomers can overcome this problem, while being able to have self-healing properties. A self-healing actuator based on liquid elastomers was developed that can mimic muscles.[46] An insect-sized robot with three legs driven to walk by low-voltage DEAs was developed in recent years and represents the only environmental stimulus actuated robot that can walk autonomously.[47]

Piezoelectric materials are defined by either their ability to produce voltage when mechanical or vibrational forces are applied or, inversely, can deform when voltage is applied. This property makes them suitable materials for actuators. However, similarly to DEAs, they require large voltages in order to function, which often is a limiting factor in their application.[48] An example constitutes a polyvinylidene fluoride-based robot that expands and contracts upon voltage application, actuating climbing and carrying operations.[49] Servomotors are some straightforward ways to achieve actuation, however their rigid components affect the flexibility of the final design. This type of actuation was used in order to achieve a swimming octopus-like robot. A silicone-based cone with nylon and steel cables attached to it was able to mimic the movements of an octopus, having the limbs actuated by a servomotor.[34]

The current technological limitations of other materials consist of low strain found in shape memory polymers (<10%)[50], the high voltage required for dielectric polymers[51], motors required for magnetic actuators[52], etc., makes soft materials good candidates for grippers.

Soft materials such as Ecoflex have been studied as electrically responsive actuators given their high actuation strain when compared to other materials (see *Figure 10)*. Given their rather low efficiency, an increase of the actuation time up to 70 s was reported. This is related to the type of coil crossing the device and conducting the electricity, with triple-coiled wire increasing the efficiency by 40%. The actuator works by volume change due to the contained ethanol phase transition embedded in the matrix. The device is characterized by high strain up to 900%, stress up to 1.3 MPa and a low density of about 0.84 g cm^{-3}.[53] An $Ecoflex^{®}$ PneuNet-like device developed to be actuated by electrical stimulation rather than pressure was able to achieve actuation times of as low as 13 seconds. The bending was enhanced by the phase transition of ethanol or acetone embedded in the flexible material when the material reached a temperature above the boiling point.[54]

1.2.4. Actuation performance

Having outlined all of the different types of designs and modes of actuation that can be utilized in order to manufacture a soft actuator, some deductions in terms of the different extents of performance each category can achieve can be drawn. Shape-memory polymers possess

limitations in their applicability as grippers due to their low strength, stiffness, heat conductivity and recovery stress.[55] Although some of these issues could be overcome by the introduction of conductive fillers, they would be unsuitable as gripper candidates since their studied size scale is well-suited for small-scale devices in the biomedical field, such as cardiovascular applications[56] and microgrippers[57] . Additionally, due to their shape-memory irreversibility they require repeated reprogramming of the temporary shape – a feature that is not feasible for soft gripper applications.[58] Similar constraints define bi-layer actuators, considering their main studied applications on a micro-scale. Consequently, 3D soft robots provide great potential in their applicability as grippers. In the context of electrically responsive actuators, they possess excellent actuation strain when compared to other materials, such as piezo polymers or DEA, as depicted in *Figure 6*. However, the efficiency of the material is rather low, which could lead to delayed actuation performance. Another limitation consists of their susceptibility to damage, a feature that is derived from their main mechanical properties that makes them desirable over rigid materials, namely their ability to be soft (low Young's modulus) and deform.

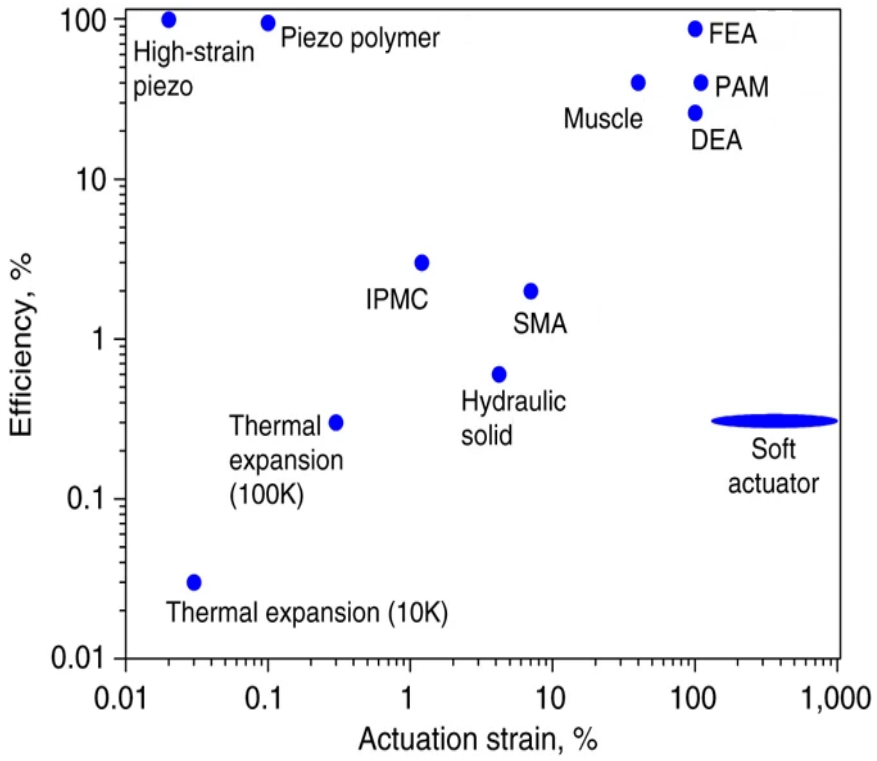

Figure 6. *Plot depicting the maximal efficiency versus actuation strain for different types of materials. Figure taken from* [53]

1.3. The self-healing effect

A major challenge associated with the use of soft robots in several applications including their use as tools in the medical industry, the packaging or fruit handling industry is their high susceptibility to damage. Their soft, flexible nature makes them prone to cuts, tears and perforations when operating with sharp objects. A lifetime reduction from 50 000 to 5000 grips was reported for the commercial robotic gripper Versaball of Empire Robotics when operating sharp objects.[59] Tendon cuts are another source of damage for soft robots that use wires for their actuation either as a result of repetitive friction during the actuation or overloading.[3] Fatigue occurs due to micro damages caused by cyclic deformation, resulting in leaks that decrease the efficiency of the actuator, at first, and sometimes leading to failure.[60] Given that a particularly challenging disadvantage that soft robotics possess is their low damage resistance, the self-healing effect present in different types of materials has been considered in various studies in an attempt to improve upon the functionality of soft-robots.

Designs that favor the reduction in stress-strain concentration can improve the lifetime of a soft robot, while at the same time limiting the freedom to explore different configurations.[61] A common soft robotic manufacturing technique is executed via multi-step molding or casting, particularly for actuators that require a hollow design. For both of the manufacturing techniques the prepolymer is poured in its fluidic form into a mold and cross-linked to its desired shape. When joining together separate parts done in different molds, those are generally glued with an adhesive or a prepolymer. This type of manufacturing technique promotes the presence of weak spots throughout the device given that the interactions between different parts are mostly physical rather than covalent bonds. Failure of the interfacial bonding is more likely to occur in this type of situations during cyclic actuations, also known as delamination.[6] Lastly, UV degradation of silicone-based elastomers and polyurethanes is another concern when it comes to preserving the properties and functionality of soft robotic materials over a long period of time, a matter that is often overlooked in robotics papers.[62,63]

Given the different types of damages that a robotic device can be subjected to, those can be divided into damages that affect the efficiency of the device and damages that result in total failure of its functionality. Currently this type of issue is resolved by replacing the component that was subjected to the damage, however, although the soft robotic specific materials are not costly, the manufacturing of the device can get costly. If a soft robot that is used in the open field fails, the damaged part needs to be replaced by either bringing the spare part at the location of failure or by transferring the robot to a maintenance spot. This process would result in delayed offline time, additional costs and non-recyclable waste components.[3]

Inspired by biology, new ways of tackling the damage that can occur to soft robots can be looked at. When the human body gets scratched or superficially cut, the soft tissue that is prone to injuries can self-heal. Manufacturing soft robots with healing abilities that mimic biochemical processes could fix the micro and macroscopic damages that occur during handling of objects, resulting in lower overall costs and more environmentally friendly products. Over the past decades the research in the field of self-healing polymers has shown to have promising applicability in diverse fields that require the restoration of damaged materials.

Self-healing materials have the outstanding property of mechanical breakage repairment.[14] Two main methods of preparing self-healing polymers can be distinguished, namely the insertion of healing agents by means of, e.g., monomer- containing microcapsules or vascular networks and the use of polymeric networks with reversible interactions, such as covalent or non-covalent interactions.[64,65] The latter can be achieved by covalent bonds, such as Diels-Alder reactions[66] or non-covalent interactions, like hydrogen bonds[67], ionic interactions[68], metal-ligand interactions. Improved self-healing was reported for polymeric materials that present shape-memory character, also known as shape-memory assisted self-healing (SMASH). If the healing mechanism is only triggered by the damage, this is called an autonomous system, while in the case where the healing requires an external stimulus such as light, heat, mechanical force etc., this falls in the category of non-autonomous healing.[3] When the material has an inherent healing ability due to chemical groups and specific properties, this is called *intrinsic self-healing*, while if the healing is incorporated by means of healing agents like the ones mentioned, they are called *extrinsic self-healing*. These categories are summarized in *Table 1*.

Table 1: Classification of different self-healing modalities in polymers[3]

Non-autonomous	**Autonomous**	
Thermoreversible covalent bonds	Hydrogen bonds	Healing agents encapsulated in:
Photoreversible covalent bonds	π- π stacking	Capsules
Exchange reaction covalent bonds	Metal-ligand (coordination) complexes	Tubes
Ionic (coordination) complexes	Mechanochemical covalent bonds	Vascular systems
High-temperature transition phase		
Intrinsic		**Extrinsic**

1.3.1. Extrinsic healing

Healing agents often work by having microcapsules containing chemical reagents stored in the matrix of the polymer, which get released upon breaking. Once they start filling the rupture, the polymerization of the monomeric agents begins and soon the liquid solidifies leaving the crack sealed.[69,70] Given the reduced size a microcapsule consists of, the healing can only be done at a microscopic level, leaving the applicability of such a process limited to instances like fatigue micro-

crack healing before they emerge into macroscopic cracks. In order to fix larger defects vascular systems or hollow fibers can be used.[71,72] There is a limited amount of healing cycles that can be carried out, given a finite number of containers that incorporate the healing agent. Healing agents best work together with brittle materials, such that the matrix is stiffer than the shell of the microcapsule. Therefore, no successful combination of healing agents with elastomeric materials has been reported.[3]

1.3.2. Intrinsic healing

Healing based on dynamic covalent bonds requires significant energy given that the bond strength can be between 150-550 kJ mol^{-1}, while hydrogen bonds require only a few kJ mol^{-1}. The high bond strength signifies substantial mechanical strength, which is a characteristic required in soft robotic applications. Another emerging consequence from the high bond strength is the non-autonomous character. Typically, energy in the form of heat or light is required in order to activate or enhance the healing process. Two different types of dynamic covalent bonds have been reported, namely reversible and exchangeable, with mechanisms that are dissociative or associative, respectively and can be depicted in *Figure 7*.[3]

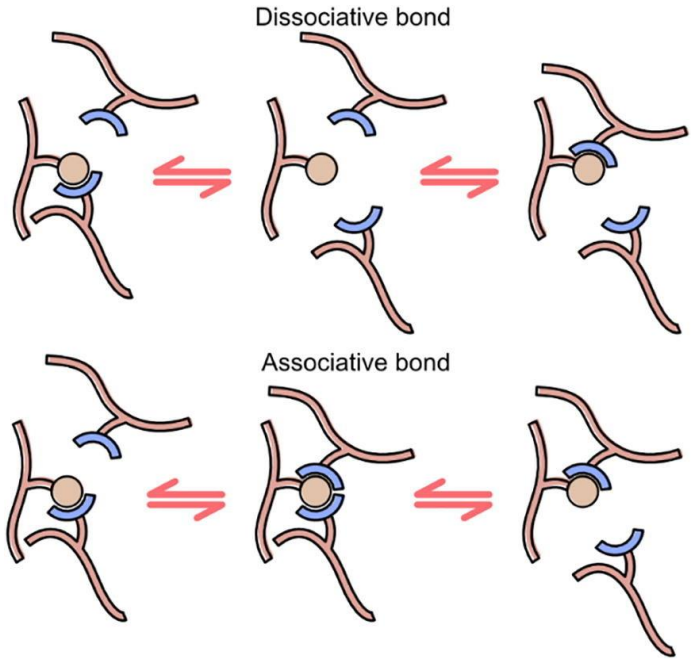

Figure 7. *Schematic representation of the two different mechanisms of dynamic covalent bonds: dissociative or reversible bonds can form and break upon the exertion of an external stimulus, while associative or exchangeable bonds can bind to new formations without suffering changes to their assembly. Figure taken from* [3]

1.3.2.1. Intrinsic dissociative covalent bonds

In order to achieve intrinsic healability, thermoreversible covalent addition reactions are often used, the most studied of all being Diels-Alder cycloaddition. The self-healing effect resulting from Diels-Alder reactions most popularly takes place between diene (furan) and a dienophile (maleimide), as depicted in *Figure 11.* The formation of the thermo-reversible cross-links allows for the cyclic self-healing process at controlled temperatures. The cycle is depicted in *Figure 8* and can be divided into five different stages: in the first stage (*Damaged*) the deterioration to the material occurs, where the DA bonds are physically broken either by cutting or perforation of the material. During the second stage the *Healing* starts by applying heat to the system (120-130℃), which shifts the equilibrium of the reaction to the rDA, where the DA bonds start to break. This results in network mobility. When maintaining the temperature constant (*Isothermal stage*), the network gains more mobility and the DA bond breakage is maximized over a period of time of 20-40 minutes. The increased mobility, thermal expansion and shape memory effect have a combined contribution in the sealing of the gap in the material created by the damage. Upon controlled cooling, the equilibrium of the reaction is reversed back to DA-bond formation, given that the product formation is an exothermic reaction. The cooling is essential to be carried out with a low gradient in order to restore the initial mechanical properties of the material.[3]

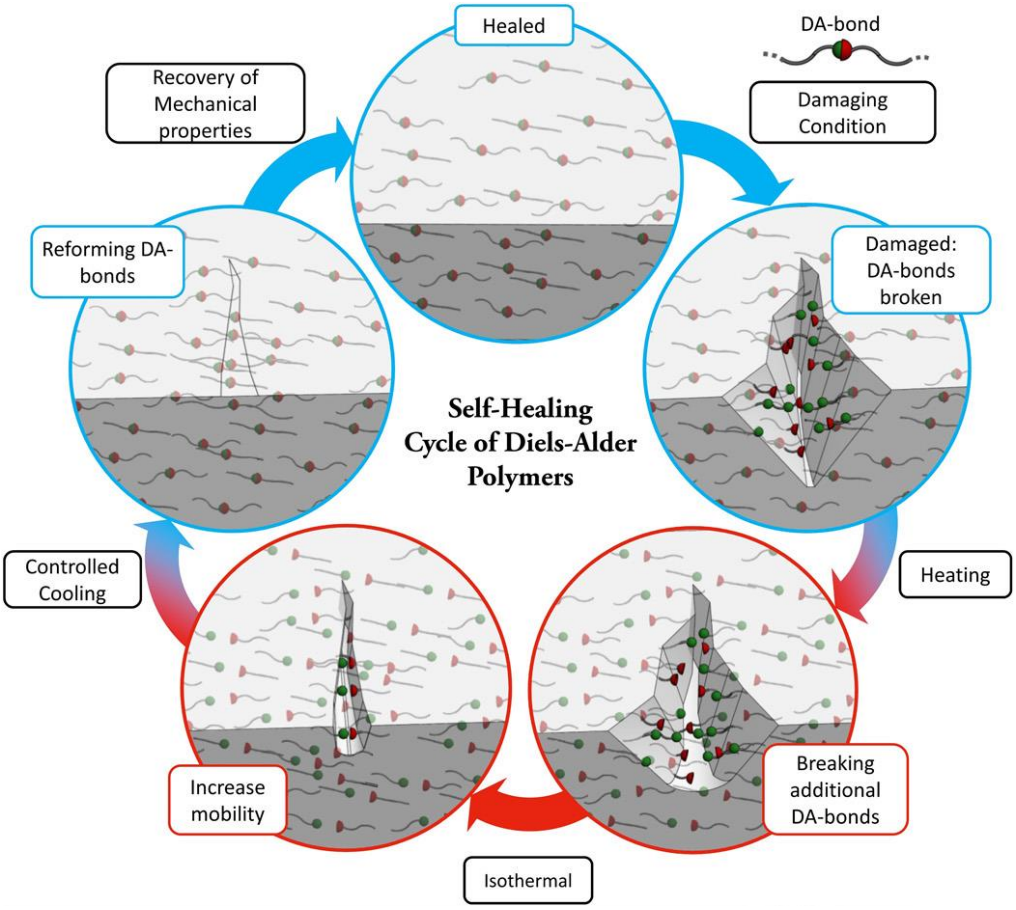

Figure 8. *Depiction of the self-healing cycle of Diels-Alder polymers. Figure taken from* [38]

Other types of intrinsic dissociative bonds are photoreversible and mechano-reversible bonds. In the case of the former, irradiation with light (e.g..: UV) acts as a fusing or breaking mechanism of bonds in certain chemical structures, such as coumarin [2+2] cycloaddition[73] and anthracene [4+4] cycloaddition[74]. However, this type of application is limited to superficial damages in the range of micrometers.[73] In the case of mechano-reversible healing, new functional groups form upon mechanical breaking of bonds which can bind again once the mechanical force is withdrawn. Studies show that mechanical breaking of DA cycloadducts results in a lower activation energy of the retro DA reaction, which suggests that DA reactions could be characterized as mechano-reversible, however there is no reported evidence that this type of healing is being studied in an elastomeric context.[3]

1.3.2.2. Intrinsic associative covalent bonds

In this category fall exchange reactions, where upon breaking of a covalent bond, a new one is formed between one of the fragmented parts and a different group. The reaction kinetics

are fastened by temperature, with a healing ability within as fast as a few hours. A few examples consist of transesterification reactions[75] with a healing time of 24 h at 80 °C, hydroxyl ester networks with a healing time of 3 h at temperatures of 160 °C. [76]

1.3.2.3. Intrinsic physicochemical bonds

To this category belong non-covalent interactions, which have a significantly lower bond energy and are therefore weaker than covalent bonds. A few examples consist of hydrogen bonds, ionomers and metal-ligand based complexes. Hydrogen bonds present a very low bond energy of a few tens of kJ/mol, meaning that a low energy is necessary in order to break them. However, due to the same reason the mechanical strength, creep and strain recovery are affected negatively. This can be tackled by increasing the number of hydrogen bonds that emerge per crosslink, leading to a self-healing ability at room temperature within a few minutes.[77] π–π stackings suffer from the same weak bond challenges, having a bond energy even lower than hydrogen bonds, limiting the strength and elastic recovery of the material.[78]

Ionic structures can be used in self-healing applications given that they can form reversible physical crosslinks. Due to their stronger bonds, they benefit from having improved mechanical properties than other physical crosslinks, often requiring an external stimulus such as heat in order to facilitate the healing process. Substantially lower temperatures are required, however, as opposed to covalent bonds, having recent studies show that autonomous self-healing can be achieved in some situations in 24 h.[79] Metal-ligand complexes belong to the same group of self-healing mechanisms, having charged metal ions form reversible physical crosslinks with the partially negatively charged groups on the ligands. Those interactions are weaker than ionic interactions given that they can be described as dipole-ion, rather than ion-ion interactions. This feature makes them healable at room temperature and reprocessible.[80]

1.3.3. Materials with self-healing abilities suited for soft robotic applications

An evaluation on the potential of the different self-healing materials to find application in soft robotic manufacturing was conducted. [3] Five different criteria were considered, as follows: 1) the ability to heal macroscopic damages, 2) the capacity to conduct multiple healing cycles, 3) recovery of initial properties, 4) possession of high strength, 5) reprocessability and recyclability. While the majority of the materials with intrinsic healing abilities meet at least four of the five assigned requirements, the ones described by extrinsic healing fail to meet half of the criteria or more. Based on this assessment, it was revealed that thermoreversible intrinsic self-healing polymers are good candidates for their applicability in soft robotics. One such type of materials

that can be described by its thermoreversibility is the class of functionalized polyketones with reversible Diels-Alder crosslinking abilities.

1.3.4. Self-healing polyketones

Polyketones are a class of polymers first synthesized in 1941 by the random copolymerization of ethylene and carbon monoxide under harsh conditions (230℃ and 200 atm).[81] Later, Reppe et al. discovered for the first time that the transition-metal catalyzed carbon-monoxide/ethylene polymerization can be carried under relatively milder conditions (200℃ and 200 atm). It wasn't until 1983 that the palladium-catalyzed reaction was discovered to give high molecular weight thermoplastic polyketones with perfectly alternating carbon monoxide/ethylene copolymers with a crystallinity of 35-50%.[81,82] The typical synthesis conditions are significantly milder, of around 90°C and 4-5 MPa. Given the high activity and yield of this type of catalyst, the same synthesis method has been used for the formation of terpolymers from carbon monoxide and other types of alkenes, one of the popular ones being ethylene/propylene/carbon monoxide terpolymers. The latter can be tuned to attain lower melting points when compared to ethylene/carbon monoxide copolymers, typically falling from 250-260 ℃ to 220 or even 170 ℃ with the addition of 6 to 17% propylene in the case of high molecular weight polyketones, making it more processible.[83] The melting point varies also with the change in chain length, lower molecular weight polyketones being described by a lower melting point. A typical example of a perfectly alternating polyketone is depicted in *Figure 9*.

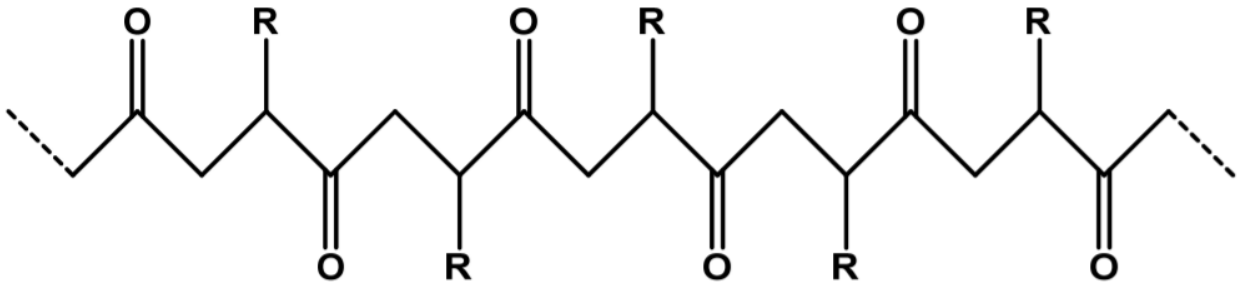

***Figure 9**. Depiction of a perfectly alternating polyketone, where R: H, CH_3, C_6H_5 etc.*

Similarly to thermoplastic polyketones, thermosetting polyketones can be synthesized by co- and ter-polymerization between carbon monoxide, ethylene and propylene in the presence of a palladium-based catalyst. Typical reaction conditions vary between 70-100 ℃ and 8.5MPa. Given the highly active carbonyl groups present on the backbone of the polymers, chemical

conversion of those types of polymers can be done by different routes, such as condensation that results in polyfurans, reduction to polyalcohols, etc.[83]

1.3.4.1. The Paal-Knorr reaction

In order to achieve self-healing properties in polyketones, a thermoreversible reaction can be tailored by functionalization and cross-linking of the original polymeric backbone. The Paal-Knorr reaction is popular when it comes to cross-linking of thermosetting polyketones and it works by forming a pyrrole ring from the interaction between an amino and two adjacent carbonyl groups, as depicted in *Figure 10.* Amino-based curing agents are used in order to form the aromatic pyrrole units with the elimination of water.[84]

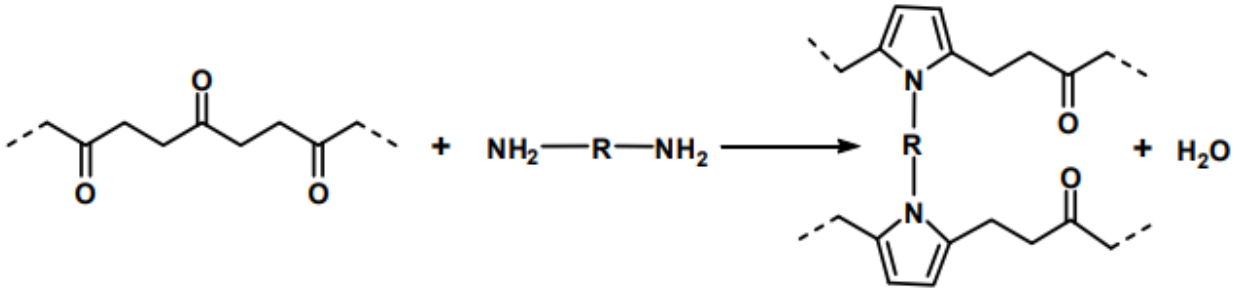

Figure 10. *Depiction of the cross-linking chemistry of thermosetting polyketones through the Paal-Knorr reaction*

1.3.4.2. Diels-Alder reaction

Shape-memory and self-healing polymers based on the Diels-Alder reaction are showing increasing interest due to their ability to be reprocessable, given the cross-linking reversibility feature that comes at elevated temperatures. DA-based cross-linked materials can be recycled and show self-healing properties, which contribute to both environmental and innovation prospects.[85]

The Diels-Alder reaction takes place between a conjugated diene and a dienophile, resulting in the formation of an alicyclic or a heterocyclic six-membered ring, where two sigma bonds form and two pi bonds get disrupted.[86] A commonly studied DA reaction in this context is the furan-maleimide (Fu/Ma) reaction, which can be depicted in *Figure 11.*[87] Similarly, in the case of polyketones cross-linked by means of the Paal-Knorr reaction described above, the pyrrole unit can react with a maleimide in order to achieve a DA adduct. The forward reaction takes place around 60℃, while the retro-Diels-Alder (r-DA) reaction takes place at 100℃ and 135℃, where

the endo- and exo- isomers are created, respectively. The final structure of the polyketone upon furan-functionalization and crosslinking with bismaleimide can be depicted in *Figure 12.*

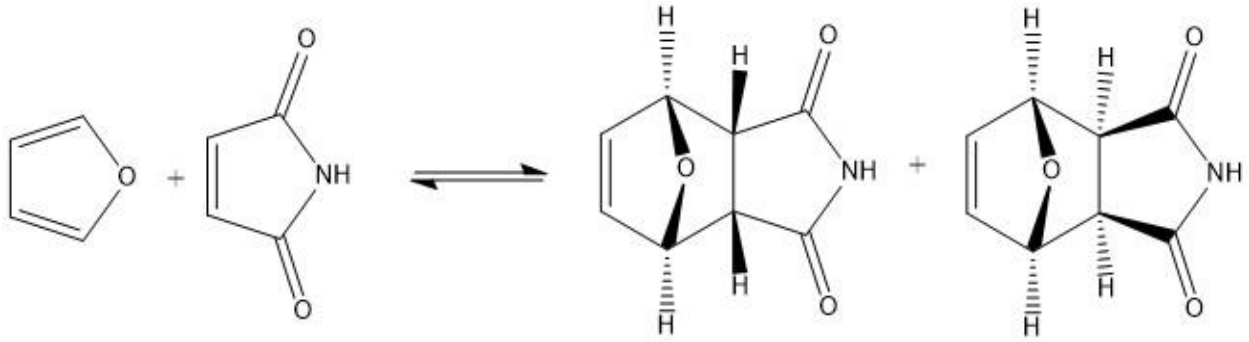

Figure 11. *The DA equilibrium reaction between furan (Fu) and maleimide (Ma) groups resulting in the endo (left) and exo (right) Fu/Ma DA adducts*[87]

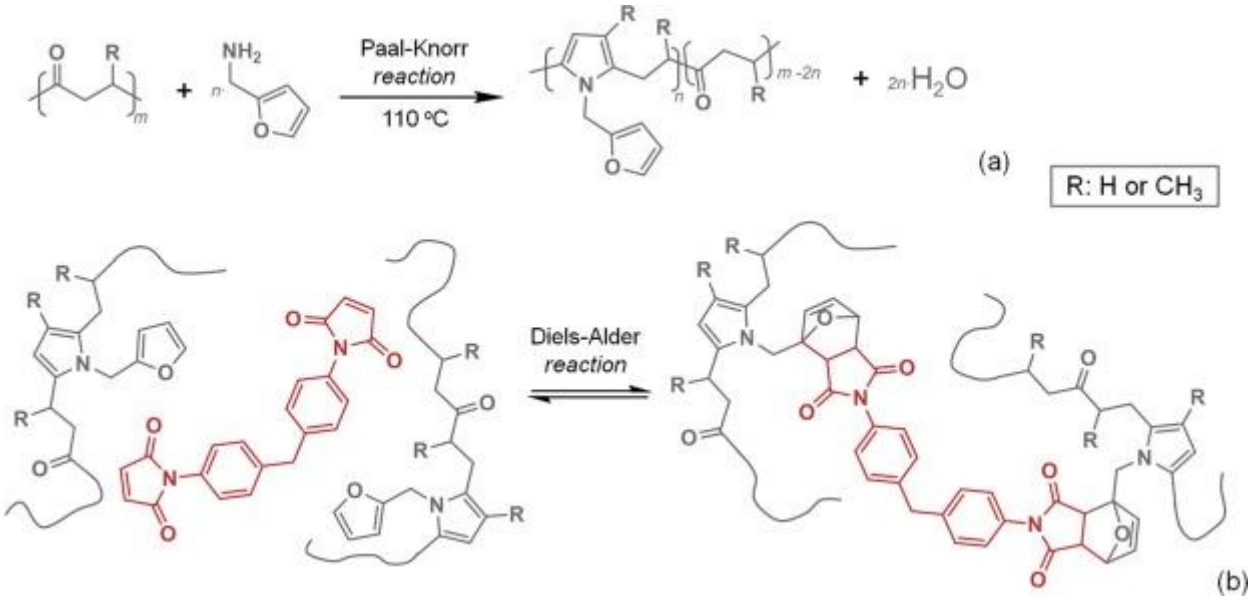

Figure 12. *a) Depiction of the Paal-Knorr reaction; b) Schematic representation of the Diels-Alder reaction. Figure taken from* [88]

1.3.5. Self-healing soft robots

This section will summarize a brief overview on the limited reported self-healing soft robots up to date. Shepherd et al. reported the manufacturing of a silicone/Kevlar soft pneumatic gripper that could restore its initial shape after a needle induced damage. [89] Although the application is best suited for occasions where superficial damages take place, the study is notable given that most damages that occur are from small perforations. A pneumatic gripper fully made out of a

self-healing polymer with a Diels-Alder healing principle was developed.[38] The healing was performed by heating up the actuator to 80 °C for about 20-40 minutes in an oven, followed by controlled cooling. An autonomously healable soft robot was investigated that would heal at room temperature in order to avoid the need to apply external heat for the self-healing process.[90] In order to obtain room temperature self-healing, high network mobility is desired, which comes with a trade-off between flexibility and mechanical strength. Zhang et al. manufactured a self-healing and shape memory polyurethane based on the Diels-Alder thermoreversible reaction by means of direct 3D printing of the polymer. [91] The external stimulus used to trigger the healing process is NIR laser irradiation.

1.4. Objectives of this work

This work aims to design a self-healing actuator that can find applications in robotic grapplers. In accordance with the literature findings, an actuator made from two different types of silicone-based elastomeric materials specific for soft robotics was manufactured, with a self-healing layer attached to the gripping side made from thermoreversible polyketones. Given that the self-healing effect of the polyketone is triggered by temperature, a device that gets actuated by (indirect) thermal stimulus is desired. An electrical conductor that produces thermal energy by means of the Joule heating effect was chosen. The device is filled with ethanol and it expands due to an increase in the vapor pressure when the liquid reaches its boiling point. Two different designs were explored, a bilayer actuator where one layer is made out of Ecoflex filled with ethanol next to a polyketone layer, and a pneumatic actuator made out of Ecoflex/Sylgard 184 PDMS + paper filled with ethanol. Detailed experimental work was carried out on the pneumatic actuator, given the faster actuation time and efficiency in repeating the actuation cycle. The working principle and a schematic of its manufacturing can be depicted in *Figure 13.*

The research questions that can be derived from this objective are: *What are the key variables that influence actuation? How could these variables be optimized? To what extent is self-healing achievable simultaneously with the actuation?*

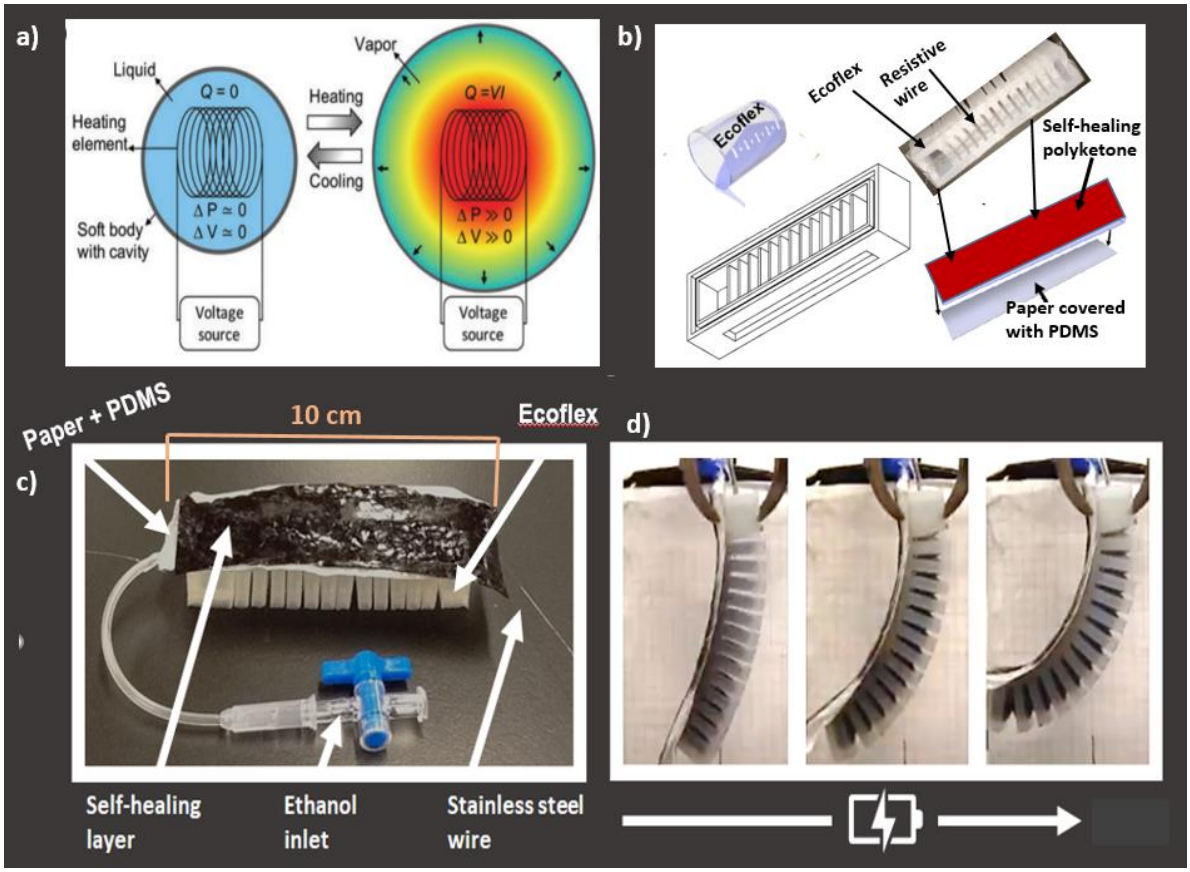

Figure 13. *a) Working principle of the device depicting the liquid phase transition; b) Assembly of the actuator; c) Depiction of the assembled actuator; d) Bending of the actuator with electricity*

2. Design

2.1. Actuator design

The device was inspired by the existing design of pneumatic actuators, made up of a series of chambers interconnected by a channel and enclosed in an extensible elastomer. Three main parameters are reported to be crucial in the fabrication of the final design: 1) the inflation rate, 2) the internal channel and external wall geometry, and 3) the choice of the material used in its manufacturing.[6] Each of these three parameters were investigated during the manufacturing of the final design and are described below.

2.1.1. Wire and liquid selection

Unlike most studied pneumatic actuators that bend upon air pressurization of the channels, the current device bends as a result of pressure build-up when electricity is passed

through the device. The electrical current (I) is transferred to a resistive coil, which generates heat. When the liquid entrapped reaches its boiling point it starts to evaporate, resulting in the volume expansion of the chambers and the bending effect of the device. In order to reverse the actuation, the electrical current is discontinued and the device cools down as a result of the heat dissipation to the surrounding.

The inflation rate is related to all three different parameters considered in the manufacturing; however, two important design parameters are the choice of the resistive wire and inflation medium. Two different wires were considered, namely a wire made of copper and a stainless-steel wire. The copper wire showed poor resistivity and heating of the material at constant voltage when compared to stainless steel, a behavior confirmed by their reported resistivity and conductivity values (*see Table 2*). Therefore, the final choice of the wire was stainless steel. In the first trials, a straight wire was passed through the device in order to obtain actuation, however, this showed poor heat distribution to the liquid due to its limited length (*see Figure A1 in the Appendix).* As a result, a coiled wire of approximately 6 times the initial length (60 cm vs 10 cm) was used (*see Figure A2 in Appendix).*

Table 2*. Resistivity and conductivity values for stainless-steel and copper*

Type of material	**Resistivity (Ω•m)**	**Conductivity (S/m)**
Stainless-steel	$6.9 \cdot 10^{-7}$	$1.45 \cdot 10^{6}$
Copper	$1.68 \cdot 10^{-8}$	$5.95 \cdot 10^{7}$

The selection of the liquid can be done by taking into account the heat required to bring the liquid to its boiling point, also known as the sensible heat (ΔH_{sen}) and the heat required to transition from a liquid to a vapor phase, also known as the latent heat (ΔH_{vap}), the latter requiring more energy than the former (*see Figure 14 a))*. Additionally, the boiling point of the liquid needs to be compliant with the desired operating temperature of the device. Considering that the Diels-Alder reaction takes place between 60-120 °C, a boiling point of the liquid within this range is desired. If the boiling point is not high enough, it could exhibit unstable behavior at room temperature and vaporize spontaneously. *Figure 14 b)* depicts a graph plotting different liquid boiling points versus their total heat. In spite of its high total heat, the liquid of choice was ethanol, due to its compliant boiling point with the functional temperature of the self-healing polymer. It was also chosen due to its safe use in contact with the outer environment in case of leakage. Carbon black was added together with ethanol in order to enhance heat distribution due to its heat and electrical conductive properties.

a) b)

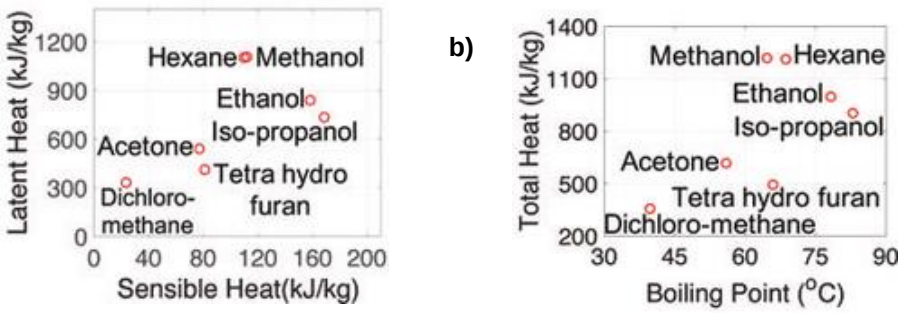

Figure 14. *a) Latent heat versus sensible heat for different types of liquids; b) Total heat versus boiling point for different types of liquids. Figure taken from* [54]

2.1.2. Design geometry

The actuator is made out of a series of expandable chambers interconnected by a channel and closed by a non-expandable, but flexible layer. The device is designed so that the chamber walls facing one another are thinner than the outside walls, with a larger surface area. This geometry ensures a preferential expansion of the interior walls with pressure build-up, with a strain minimization on the outside walls. Another important design detail is the close proximity of the neighboring chambers. As the inner walls of the chambers expand, they press against each other, resulting in the bending effect towards the side of the inextensible layer. Previous design attempts reveal the importance of close chamber proximity in the bending actuation (*see Figure 3A in the Appendix).* Overall, the length change of the extensible layer is expected to be <1%, which is preferred over a high-volume change, since the latter would require a pressurization of the device over a longer period of time in order to achieve good bending.[6]

Three different parameters were previously investigated by Mosadegh et al. on their effect on the optimization of the final design, namely the number of chambers, their height and thickness (*see Figure 15)*[6]. It was observed that an increase in the bending motion is favored by an increase in the number of chambers for a predefined length together with a decrease in the inside wall thickness. The material properties and the resolution of the 3D printer used for the mold fabrication pose limitations in the extent to which those properties can be investigated. It was shown that there is a limit over which increasing the chamber height does not contribute to improved actuation. Instead, it would negatively impact the actuation by making the device heavier, while requiring a higher amount of elastomer.

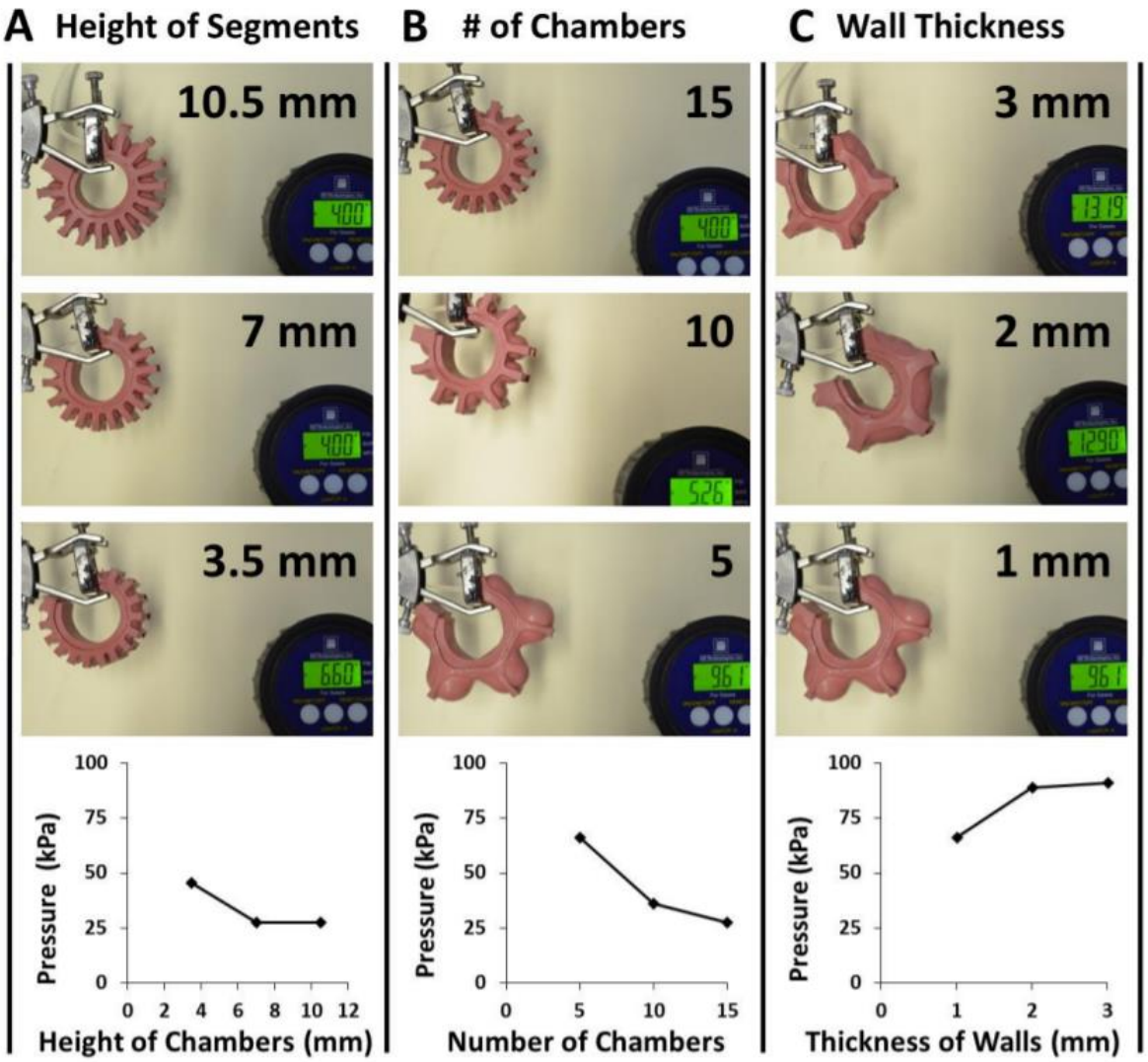

Figure 15. *Optimization of A) the segment height, B) number of chambers and C) wall thickness and the reported pressure required in order to achieve full bending for each of the varying parameters (A to C). Figure taken from* [6] *Supplementary Information*

The final design was inspired by the optimizations described and published by Mosadegh et al., with minor adjustments on the size of the interconnecting channel and the volume of one of the side chambers.[6] Two molds were printed by an 3D printer model Ender 5 pro using polylactic acid (PLA). An interior and an exterior mold were prepared in order to form the extensible layer, as depicted in *Figure 16,* while a Teflon boat was used in order to close the device with the inextensible layer. An interconnecting channel is present on the interior mold with a role in ethanol distribution throughout the device. The size difference between the interconnecting channels and the chambers (2.5 mm vs 9 mm) results in the preferential inflation

of the chambers when pressurized. The exterior mold consisted of parallel plates through which the interior mold chambers could be inserted. This ensures that each chamber has its own interior walls separated from the others. This length, height, thickness and number of chambers were chosen according to previous literature optimizations and printing limitations in terms of minimum chamber thickness (see *Figure 15),* and are equal to 93 mm, 9 mm, 1 mm and 14, respectively. One of the side chambers was adjusted to having a bigger volume in order to ensure sufficient space for both the clamping during experimental work and for the introduction of the valve through which ethanol would be added.

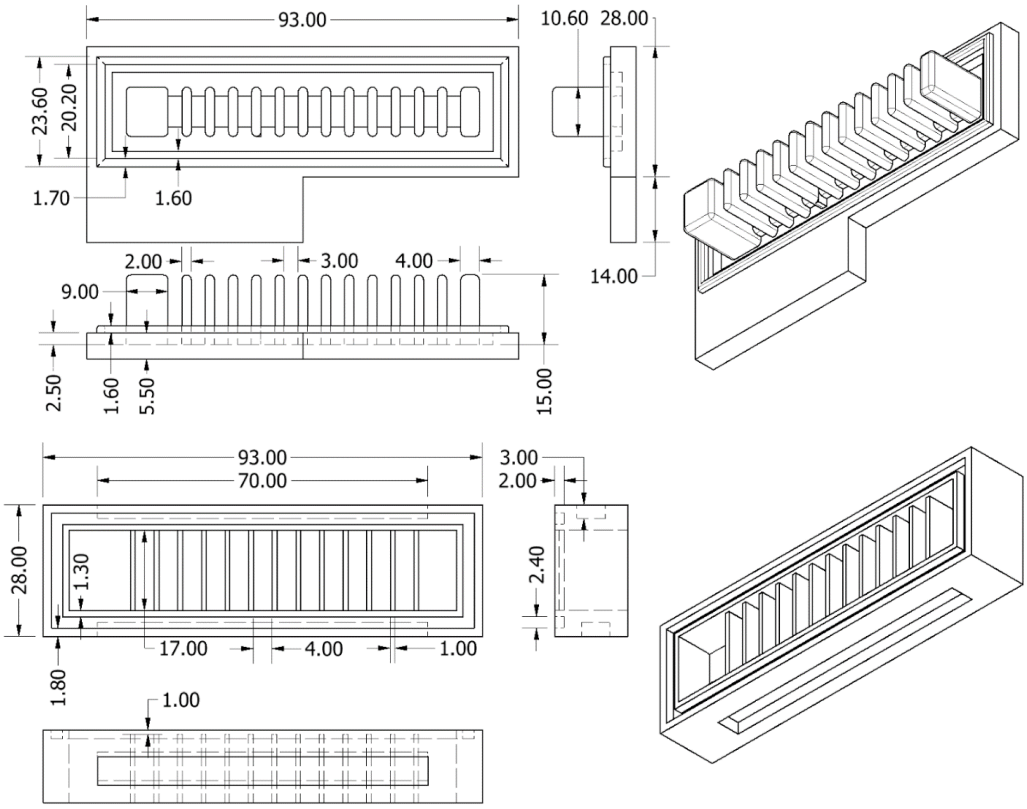

Figure 16. *Depiction of the interior and the exterior 3D printed molds used and their corresponding dimensions*

2.1.3. Material selection and assembly of the actuator

Two different types of silicone-based elastomers were used in the manufacturing of the device, considering the previously mentioned requirements for an extensible and an inextensible part. Previous investigations[6,37,92] suggest that two good candidates for the two different components are Ecoflex (00-30 / 00-50) and Sylgard 184, respectively. Their mechanical

properties differ considerably and were summarized in *Table 3*. The low Young's modulus characterizing Ecoflex 00-50 and its high tensile strength makes it and excellent candidate for the extensible layer, while the considerably higher Young's modulus and low tensile strength of Sylgard 184 are good indicators of its suitability as a non-expandable, but flexible layer.

Table 3. *Mechanical properties of Sylgard 184 and Ecoflex 00-50*[93]

Name elastomer	Young's modulus (MPa)	Ultimate tensile strain (%)	Ultimate stress (MPa)
Sylgard 184	2.4	135.6	7.1
Ecoflex 00-50	0.1	859.7	1.7

Ecoflex 00-50, Smooth-on, Inc. was used for the fabrication of the device chambers, enclosed by a thin layer of cellulose embedded in Sylgard 184 polydimethylsiloxane (PDMS) and a polyketone layer with self-healing abilities (*see Figure 17)*. Ecoflex is a soft, translucent silicone-based elastomer (00-50 Shore hardness) that can withstand repeated deformation and bending, while having a high maximum strain (860%).[93] Sylgard 184 has a significantly lower elastic modulus of up to 20%, making it a good candidate for the non-extensible layer.[94] Given the high tensile strength (approx. 50 N mm^{-2}) that cellulose paper possesses, the extension of Sylgard 184 is reduced further when incorporated in the passive layer of the actuator. The tailoring and incorporation of the paper sheet into the bottom layer is facilitated by its decreased weight (approx. 68 g m^{-2}).[39]

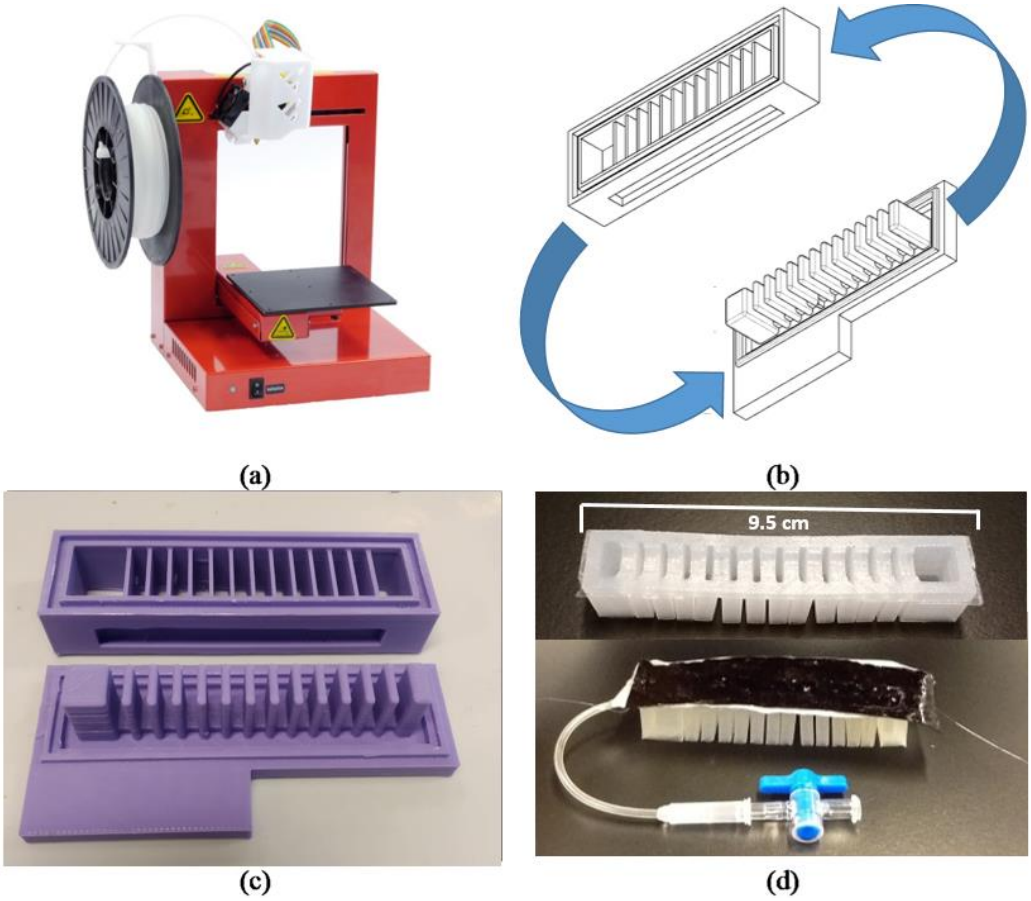

Figure 17. *a) Depiction of a 3D printer; b) schematic of the molds and their assembly; c) 3D printed molds; d) final design of the device*

The materials were prepared according to the instructions delineated by the producers, as follows: Ecoflex 00–50-part A and part B were mixed in equal ratios by mass for 1-2 minutes, followed by degassing, casting into the molds and curing for 3 hours at 50 °C. PDMS was prepared by mixing the base agent and the curing agent in a ratio of 1:10, followed by degassing and curing at room temperature for 24 hours or at 60 °C for 4 hours.

After curing, the top part of the device was carefully removed from the molds, obtaining a hollow series of chambers as depicted in *Figure A4* in the *Appendix*. A 60 cm coiled stainless-steel wire was placed on top (*see Figure A2 in the Appendix).* The assembly was then placed over of the bottom layer. The bottom layer was prepared by covering a section of paper placed in a Teflon boat with a thin layer of Sylgard 184 PDMS solution before curing. The hollow series of chambers obtained from the 3D printed molds was placed over the bottom layer facing down, together with the stainless-steel coil positioned in between the chambers and the bottom layer and left to cure, obtaining the device depicted in *Figure A5* from the *Appendix*. Next to the added

rigidity to the bottom layer, the use of paper ensured that the interconnecting channel would remain free of excess Sylgard 184 PDMS material, while improving the adhesion between the extensible and the inextensible materials. A valve was inserted into the chamber with the highest volume by first puncturing it with a tooth pick, followed by stretching of the chamber and careful insertion of the tubing connected to the valve. Additional uncured Ecoflex 00-50 was applied around the punctured area surrounding the tube and was left to cure in the oven at 50 °C for 3 h. Lastly, once all of the silicone elastomer layers were cured, the polyketone layer prepared as described in the following section was glued over the bottom layer by applying extra uncured Sylgard 184. The fully assembled device was placed in the oven at 60 °C for 4 hours in order to complete the last curing step.

2.2. Preparation of the self-healing material

The alternating polyketones with 30% ethylene content (PK30, MW: 5362 g/mol) were used as obtained from the manufacturer (Shell). Furfurylamine purchased from Sigma Aldrich with a purity of ≥ 99% was subjected to distillation before use. 1,1'-(methylenedi-4,1-phenylene)bismaleimide (check purity) and chloroform (HPLC grade) were used as purchased from Sigma Aldrich. The polyketones were prepared based on the procedure described previously by Zhang et al. [95]

2.2.1. Polyketone functionalization via the Paal-Knorr reaction

The functionalization of the polyketones was carried out with furfuryl amine via the Paal-Knorr reaction. The molar ratio between the reactants was calculated such that the maximum carbonyl conversion is equal to 20%. The reaction was carried out in a round-bottomed glass reactor equipped with a U-shaped anchor impeller, a reflux condenser and an oil bath with a role in the heating of the elements. The solvent of choice accompanying the reaction was chloroform in which PK30 was first dissolved and brought to the operating temperature of the reaction. The furfuryl amine was added dropwise for about 10 minutes. The reaction was carried out at an operating temperature of 110 °C and a rotational speed of 500 rpm for approximately 4 h. After 4 hours, a change in the appearance of the reaction contents was observed from colorless to brown due to the pyrrole unit formation on the backbone of the polymer. The obtained modified polymer was washed five times with 250 ml of deionized Milli-Q water in order to ensure the removal of the unreacted furfurylamine. The obtained solution was drop casted over two Teflon boats and allowed to dry at room temperature over the course of 3 days in order to evaporate a significant amount of the solvent. In order to fully dry the samples, a notice of their weight prior and after

drying in a vacuum oven at 70 °C overnight was taken, and the procedure was repeated until no further mass loss was observed.

2.2.2. Crosslinking via the Diels-Alder reaction

The crosslinking reaction of the functionalized polyketones was carried out using bis-maleimide in a ratio of 1:3 maleimide:furan on a weight basis, dissolved in chloroform with a 10 wt% polymer basis. The reaction was performed in a round-bottomed flask at 50 °C for 24 h at 500 rpm. The solvent was removed in a vacuum oven and followed a similar procedure to the drying of the functionalized polyketones described above. The final cross-linked polyketone layer was removed from the Teflon boat and used as obtained when the thickness low enough and homogeneous, otherwise it was subjected to compression molding in order to obtain a thin and uniform polyketone layer. An example of such a layer is shown in *Figure 18.*

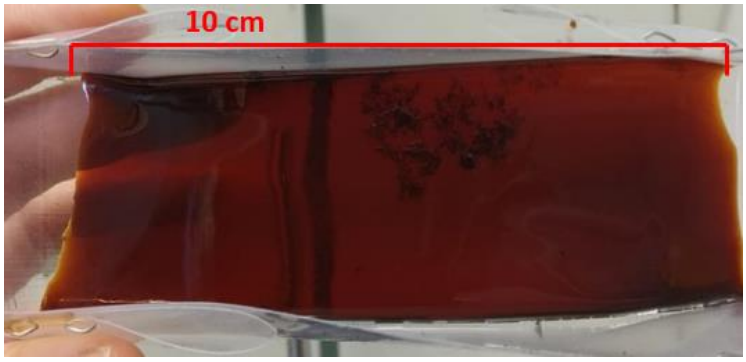

Figure 18. *Depiction of a drop-casted cross-linked polyketone layer*

2.3. Selected materials and entrapped liquid compatibility

Given that Ecoflex-50 is permeable to gases and liquids, periodic refilling of ethanol was required in order to maximize actuation. Liquid permeability of different organic solvents through PDMS was previously reported in literature and is summarized in *Table 4.*[96]

Table 4. *Summary of the liquid permeability values for different organic solvents through PDMS at 40 °C*[96]

Name of the solvent	**Permeability** ($1 \cdot 10^{-7}$ cm^3 (STP)·cm / (cm^2·s·cmHg)
Water	23
Ethanol	45
Methylene chloride	165
Chloroform	283
Carbontetrachloride	180
1,2 - Dichloroethane	248
1,1,1 - Trichloroethane	247
Trichloroethylene	614
Toluene	1460

From all the reported organic solvents, water has the lowest permeability at 40 °C, succeeded by ethanol. Leemann et al. plot the permeability of different solvents as a function of temperature (*see Figure 19).*[97] As it can be observed, although the permeability of water at room temperature is lower than that of ethanol, as temperature rises over 80 °C, its permeability exceeds that of ethanol. The permeability of all liquid solvents tested is observed to decrease with the increase in temperature.

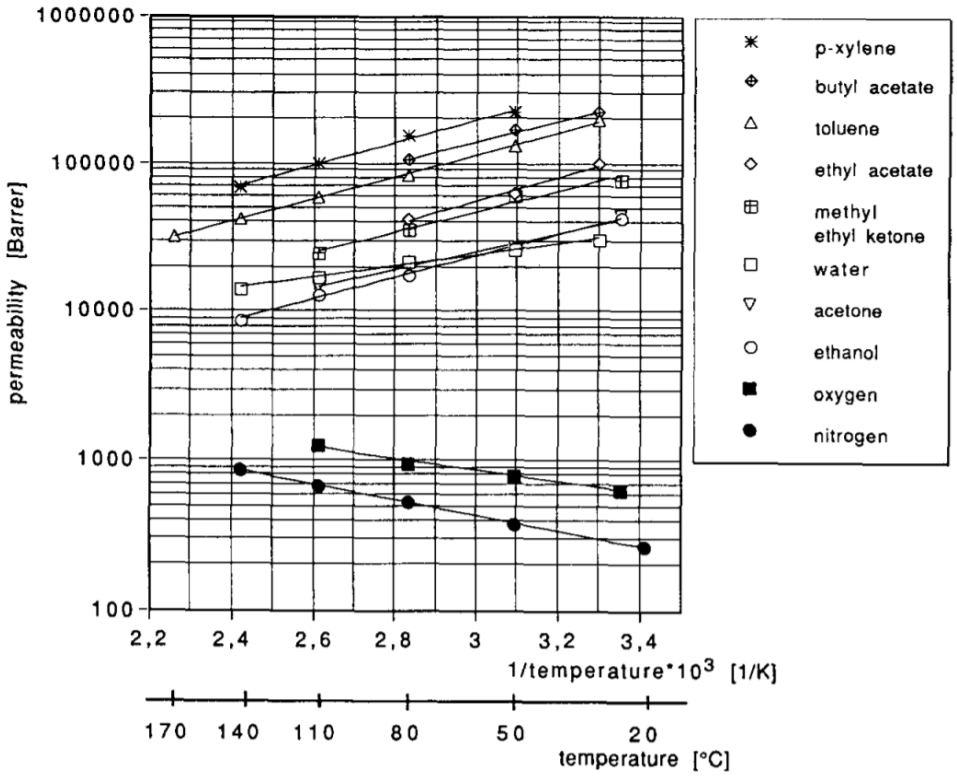

Figure 19. *Dependence of permeability for different solvents through PDMS and gases on temperature variation. Figure taken from* [97]

Although reports analyzing gas permeability state that the free volume of PDMS is temperature dependent, meaning that at higher temperatures the free volume and polymer chain mobility increase and, together with those, permeability as well[98], the effect that the increase in temperature has on the permeability of PDMS for organic solvents is reversed. However, the increase in the partial pressure of the solvent results in an increase in the degree of swelling of the polymer, and, simultaneously, an increase in the diffusivity of the solvent (*see Figure 20)*, a trend more pronounced at temperatures below 80 °C.

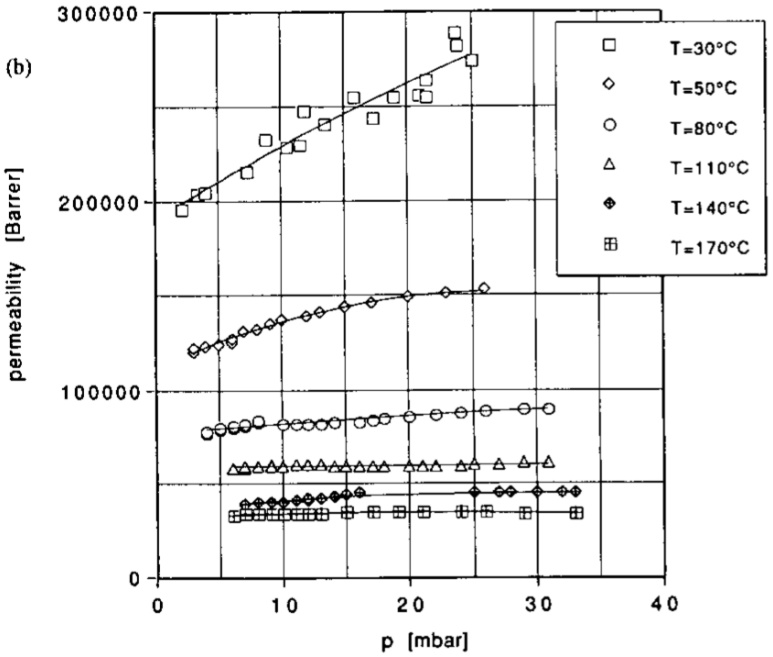

Figure 20. *Permeability of toluene through PDMS as a function of partial pressure at different temperatures. Figure taken from* [97]

The analyzed literature data suggests that the compatibility between ethanol and the silicone-based elastomer is considered to be satisfactory when compared to other organic solvents.

2.4. Characterization of the actuator

The performance of actuator with different varying parameters was tested by measuring the bending angle. The bending angle was measured using the method reported by Terryn et al., depicted in *Figure 21.*[38]

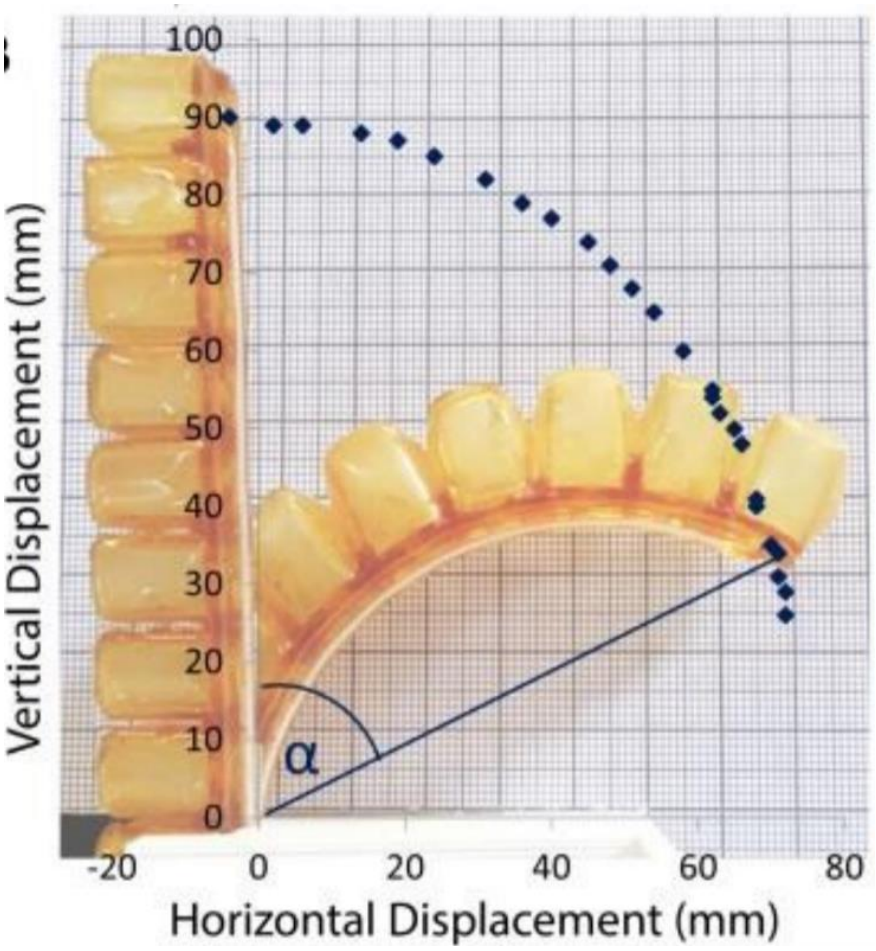

Figure 21. *Illustration of the method used to determine the bending angle during actuation*[38]

The temperature variation during the actuation was captured by a visual IR thermometer Fluke VT02. The electric current was generated using a DC power source model Velleman LABPS6005SM. The pressure build-up inside of the actuator was measured using a pressure sensor A.E. Sensors B.V.

A depiction of the set-up used throughout the experimental work can be depicted in *Figure 23.* The self-healing tests were performed by making micro-cuts of varying thicknesses into the polyketone layer using a scalpel blade and pictures of the scars were recorded before and after the actuation under a digital microscope model Keyence VHX-7000.

Figure 22. *Depiction of the set-up used during the experimental work*

Different parameters were varied throughout the experimental work in order to observe the changes in the bending angle over time. The standard devices used in all the experiments were prepared using a 60 cm long coiled wire, while the standard voltage was approximately 24.5 V, unless specified otherwise. First, the amount of ethanol was varied and the change in bending angle and temperature were recorded. Then, a constant amount of ethanol was chosen while varying the amount of carbon black added, tracking the bending angle over time and the variation in temperature. At constant amounts of ethanol and carbon black, the change in bending actuation with different power inputs were tested, along with the change in temperature. Two different wire lengths were chosen and investigated on their effect on the actuation. Lastly, the pressure build-up over time and the corresponding temperature were recorded and plotted for both pristine and pre-heated conditions.

3. Results and discussion

3.1. Ethanol variation

The amount of ethanol was varied throughout the experimental work in order to assess its effect on the bending angle as a function of time. When the device contains only air, there is hardly any actuation over the time period of 3 minutes. As soon as some low amounts of ethanol are inserted into the device, the bending angle starts raising. This is due to the increase in the vapor pressure of the liquid added. The general trend observed in *Figure 23* shows that the bending angle increases with the increase in the ethanol content, particularly after two minutes. This is considered to be the time it takes for ethanol to reach high enough vapor pressures. In contrast, there is a slight decline in the bending angle during the first minute with the increase in the mass of ethanol above 3 g. *Figure 24* showing the temperature profile with the increase in ethanol content explains the underlying reasons behind this phenomenon. Although the temperature profile increases at first with the addition of low amounts of ethanol (> 3 g), this trend shows a decline when more ethanol is added to the device. This can be explained by the specific heat of ethanol expressed in J/ (kg · K): the higher the volume of ethanol, the more energy is required to bring the liquid to its boiling point. However, once the liquid reaches temperatures high enough for its vapor pressure to increase significantly (between 100 – 150 °C), a rapid increase in the bending angle can be observed.

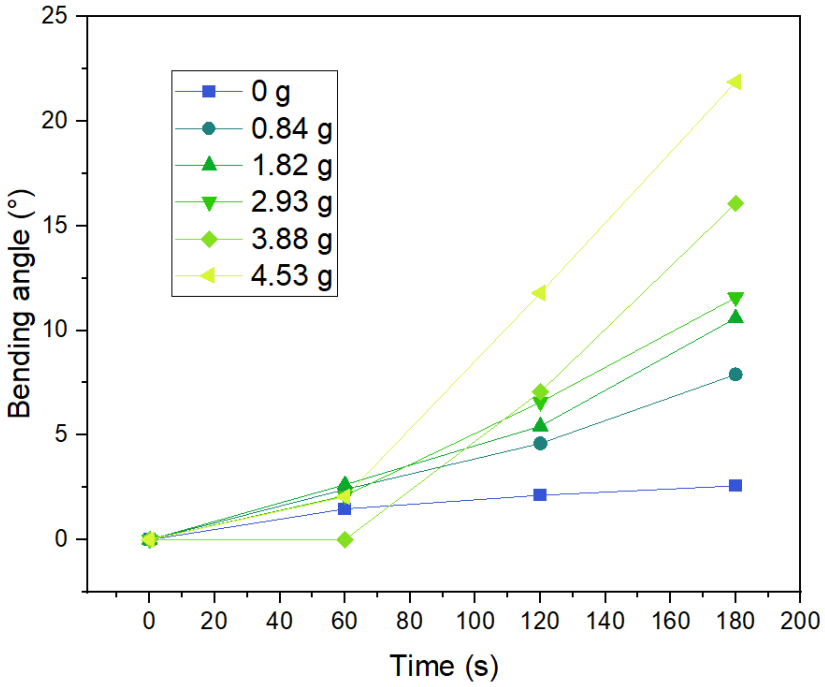

Figure 23. *Depiction of the variation in bending angle over time for different amounts of ethanol within the device*

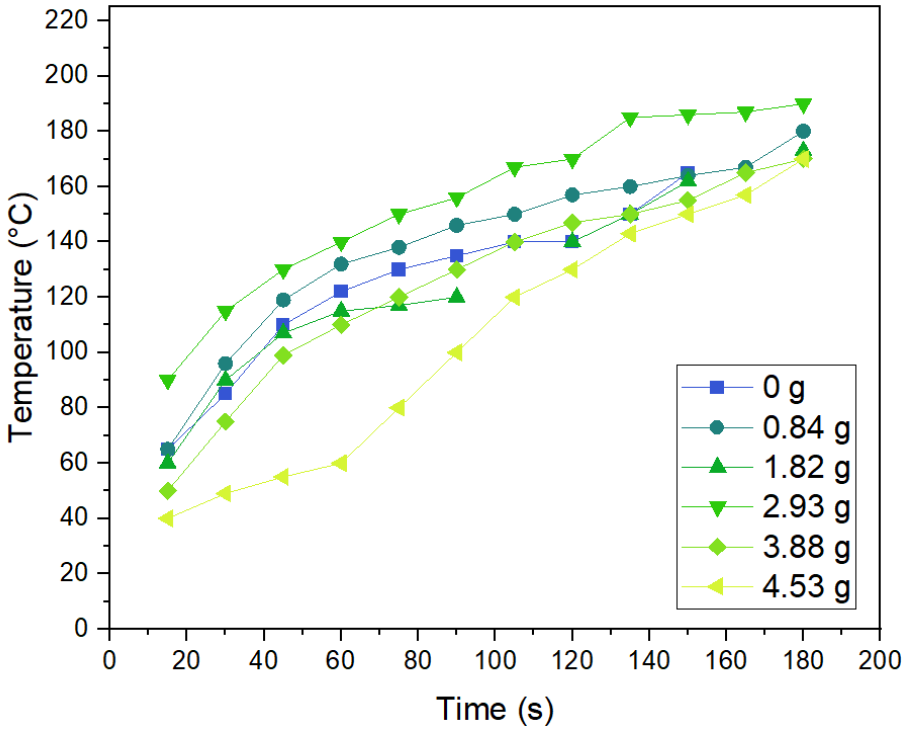

Figure 24. *Depiction of the variation of the temperature profile with the amount of ethanol within the device*

Chellattoan et al. studied the performance of an actuator with a similar design as the one described in this work, using the phase transition of ethanol or acetone as the driving pressure.[54] They use 2.5 mL of liquid throughout all of their performed experiments and reach good bending actuation in less than 10 s. The main difference is that their device is not entirely hollow, since they add a flexible heating element within the free space. Kang et al. developed a multi-layer soft robotic actuator consisting of an elastomeric matrix, a nanofiber mat with a role in the homogeneous dispersion of ethanol, a blocking and a passive layer.[99] The device uses 0.95 g ethanol and reaches full bending motion in 120 s. Other authors studying the actuation of soft robots using phase transition of ethanol design their devices using elastomers containing 20% ethanol liquid droplets with actuation times higher than 60 s.[53,100] Considering that the amount of Ecoflex 00-50 per mold used in this work is approximately 20 g, it could be stated that the highest mass of ethanol tested accounts for approximately 20% of the total weight. There is a clear difference between the two different approaches, however, since one incorporates 20% ethanol into the elastomer matrix, while this work fills up the device with 20% ethanol of the total actuator weight.

3.2. Addition of carbon black

Considering that the heating of the device is slower in the first minutes with the increase in the amount of ethanol (see *Figure 23)*, carbon black was added together with ethanol in an attempt to fasten the heating process in the first 2 minutes. The effect the addition of carbon black has on the bending angle over time was recorded and can be summarized in *Figure 25.* The amount of ethanol is kept constant at 5 g throughout the tested experiments, while varying the amount of carbon black. While it is challenging to notice a clear increase in the bending angle with the addition of carbon black after 60 seconds, a more pronounced increase can be observed after 120 seconds for all of the tested added amounts of carbon black. It is, however, difficult to observe a clear increasing trend in the bending angle with the increase in the amount of carbon black. A major cause for this could be the fluctuation in voltage throughout the experimental work. The highest values reported at 20 mg carbon black showed the best stability in terms of voltage consistency, while registering a slightly higher value than the rest of the tested experiments (24.1 V versus 23.6-23.9 V). Another reason could be due to the close proximity of the results. Considering that the measurement error accounts for 1-2 °, the slight difference is to be expected even when repeated the same experiment. Although it is unclear to what extent the variation in the amount of carbon black contributes to the speed of actuation, it is shown that it does have a significant effect after 120 s when compared to the control sample. Other attempts in carrying out similar tests can be summarized in *Figures A6 and A7* from the *Appendix.*

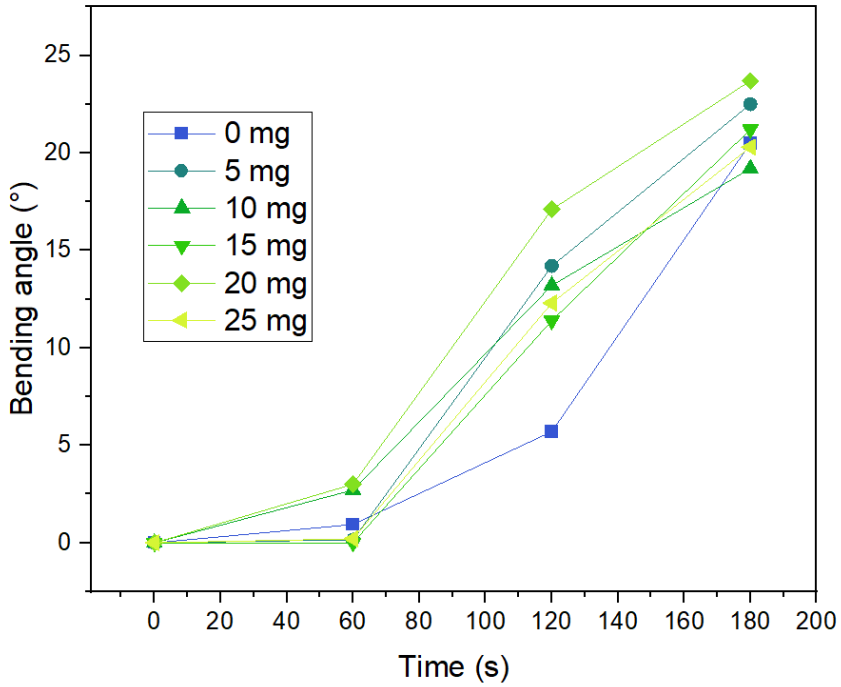

Figure 25. *Bending angle as a function of time for different amounts of carbon black*

Different approaches to enhance the heat transfer or heat distribution in soft robots actuated by phase transition have been reported. Chellattoan et al. use flexible steel microfibers as a heating element inside of a pneumatic actuator driven by ethanol phase transition and achieved actuation in less than 10 s at 45 W.[54] The multilayered actuator developed by Kang et al. uses a non-woven nanofiber mat in order to ensure homogeneous ethanol distribution, which leads to uniform actuation, with full bending in 120 s.[99] This is achieved due to the wicking effect and capillary impregnation of the mat along its entire surface.

3.3. Effect of voltage

Different voltages were tested on their effect on the bending angle of the device over time, while keeping track of the temperature profile. The amount of ethanol and carbon black were kept constant throughout the experiments. A trend of increasing bending angle with the increase in the voltage can be depicted in *Figure 26.* The temperature profile suggests that a contributor to this trend is the increase in temperature as the power input is raised. The time needed to reach the boiling point of ethanol can be adjusted accordingly by increasing the voltage/ power input. As shown in *Figure 27*, when increasing the voltage from 25 to 35 V (equivalent to power inputs of 11.3 and 22.4 W, respectively), the time required to reach the boiling point of ethanol decreases from 90 to 40 s. It can be observed that the temperature profile increases rapidly after the first 60 s at higher voltages, however it shows slow increase in the first 60 seconds. Although there is an improvement in the bending angle after 60 seconds with the increase in voltage, this remains rather low before reaching 120 s voltages in the 20-30 V range. However, when the voltage is increased over 30 V, a rapid increase in the bending angle from the first 20 s can be observed. Elevated temperatures are reached in very short times, going up to over 200 °C in less than 90 s.

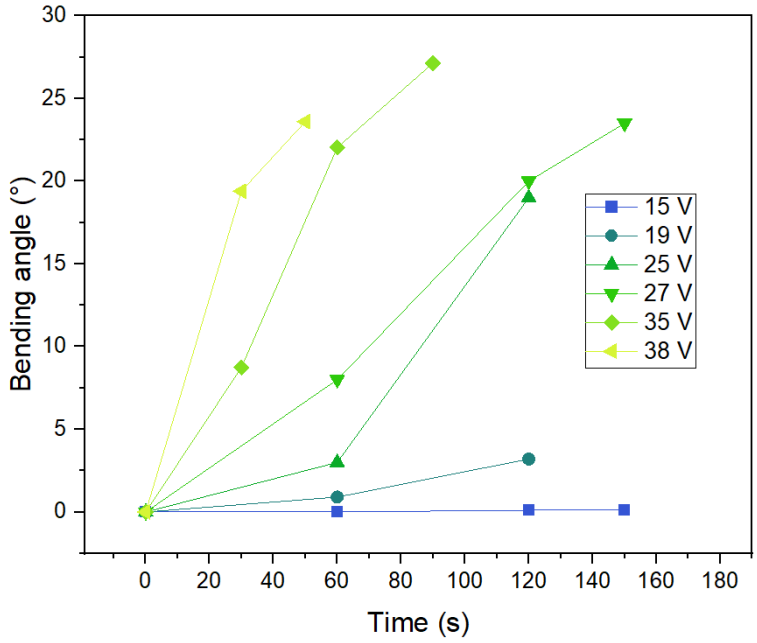

Figure 26. *Bending angle as a function of time at different voltage inputs*

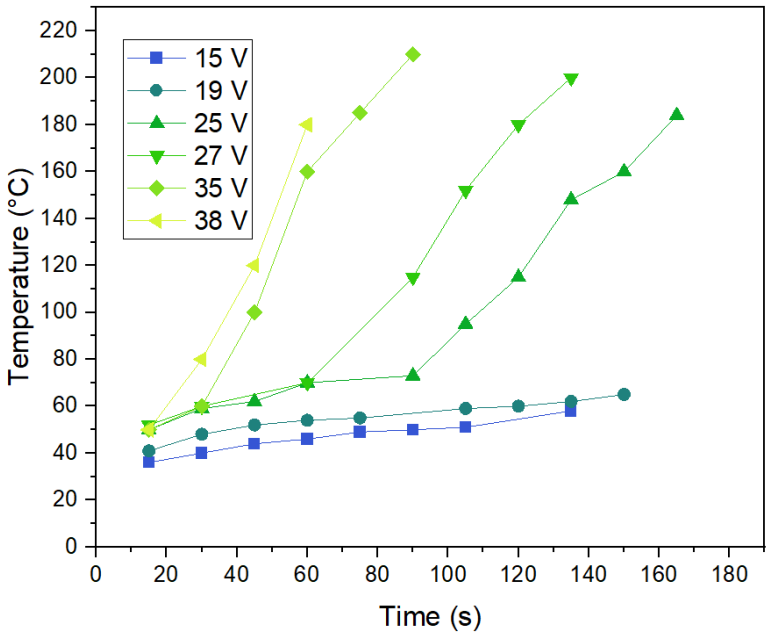

Figure 27. *Temperature profile as a function of time at different voltage inputs*

Chellatoan et al. demonstrated fast deformation (under 1 minute) of a pneumatic actuator driven by ethanol phase transition when powering their device at 30-45 W.[54] Miriyev et al. designed a McKibben-type of muscle that is actuated with ethanol phase transition powered at 45 W and a bilayer actuator working by the same principle powered at 8 W, achieved in over 1 minute.[53] The data suggests that the power range the current device was tested at is similar to

the ones reported in literature for low-voltage soft actuators. The response time could facilitate from further improvements, as discussed further.

3.4. Wire length variation

The change in the bending angle over time was recorded for two different devices using different coil lengths. The tests were carried out using two different amounts of ethanol, as it can be depicted in *Table5.* The bending angle does not differ significantly when comparing a device using a wire length of 37.5 cm versus one composed of a 60 cm wire. Considering a bending angle measurement error of 1-2°, it can be stated that for most of the data points the bending angle is approximately equal for both of the tested devices. In contrast, a difference can be observed in the value of the current and the resulting overall required power. The device with a shorter wire length requires more current when compared with the one with a longer wire. The resulting overall extra power input required for the 37.5 cm wire device is about 3-4 W.

Table 5. *Summary of bending angle and power input for different wire lengths*

4.53 g Et-OH	37.5 cm				60 cm			
Time (s)	Bending angle (°)	Voltage (V)	Current (A)	Power (W)	Bending angle (°)	Voltage (V)	Current (A)	Power (W)
60	2.7	24.2	0.55	13.3	2.05	24.4	0.42	10.25
120	7.9	24.1	0.55	13.3	11.8	24.4	0.42	10.25
180	23.3	24.2	0.55	13.3	21.9	24.4	0.42	10.25

1.82 g Et-OH	37.5 cm				60 cm			
Time (s)	Bending angle (°)	Voltage (V)	Current (A)	Power (W)	Bending angle (°)	Voltage (V)	Current (A)	Power (W)
60	2.6	24.5	0.58	14.21	2.63	24.4	0.41	10
120	6.3	24.5	0.58	14.21	5.42	24.5	0.42	10.29
180	11.2	24.5	0.58	14.21	10.59	24.7	0.42	10.37

3.5. The influence of pressure build-up on the bending angle

The bending angle and temperature profile were recorded as a function of the pressure build-up inside of the device. As it can be observed in *Figure 28,* there is a steady increase in the pressure build-up with the bending angle, which is to be expected considering that the driving force that causes the motion of the device is the overpressure forming as a result of the vapor pressure increase of ethanol at elevated temperatures. The pressure build-up is therefore facilitated by the increase in temperature and it can be observed that this starts raising well before ethanol reaches its boiling point. The highest overpressure reached over the standard time used throughout all of the experiments (180 s) was 9 kPa, for a composition of 4.62 g ethanol and 35.3 mg carbon black. It is worth noting that at different compositions of ethanol/carbon black, elevated

temperatures could be reached sooner. However, based on the experimental observations, that does not necessarily correspond to higher bending angles or pressure build-up.

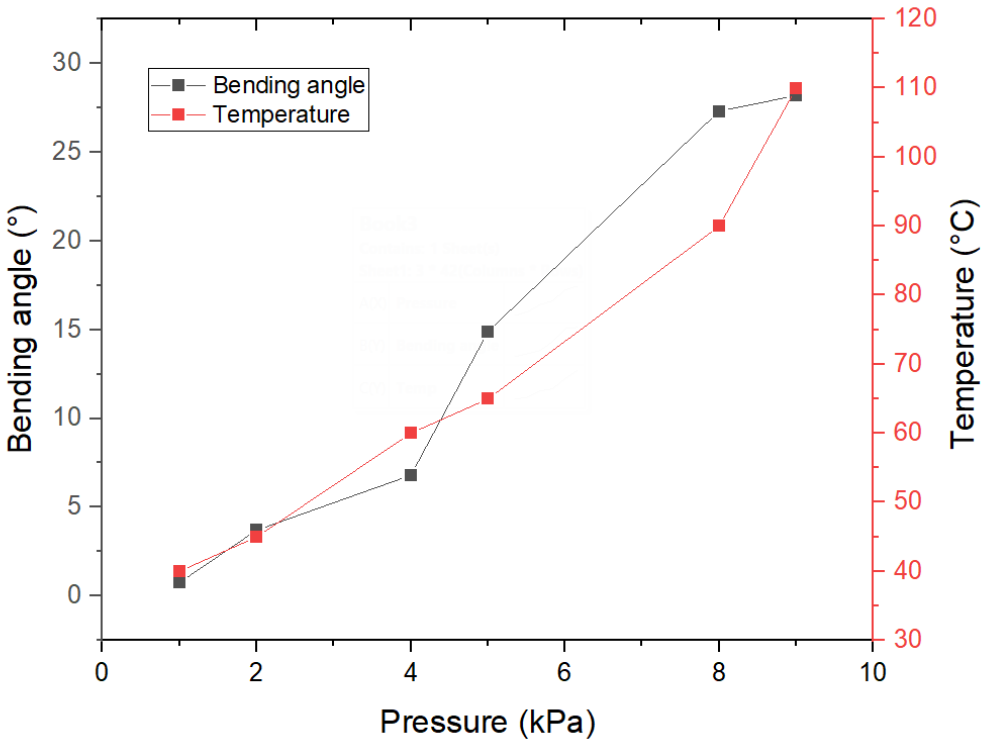

Figure 28. *Bending angle and temperature profile as a function of pressure build-up inside of the device*

Terryn et al. reported the bending angle exerted by different self-healing pneumatic actuators tested as a function of the overpressure (*Figure 29 a)*.[38] The mechanical properties of the material used in the fabrication of those is somewhat comparable to the ones of the materials used in this work (ultimate stress 1.8 vs 1.7 MPa; ultimate strain 356 vs 860%). Two of the devices have a wall thickness of 0.75 mm (SPA 1 and SPA 2) and the others (SPA 3 and SPA 4) have a wall thickness of 0.6 mm, both of them lower than the wall thickness of the device used in this work (1 mm). As it can be observed in *Figure 29 b*, the bending angle that corresponds to overpressures that coincide with the range exhibited in this study is similar to the bending angle recorded in this work. Although in the range of 1-5 kPa the bending angle of the current device is lower than the ones depicted in Terryn et al.'s work, this starts raising rapidly once the pressure inside the actuator reaches values above 5 kPa. This could be linked to the device approaching temperatures close to the boiling point of ethanol, therefore rapid pressure build-up and more pronounced bending response. Overall, the data suggests that the performance of the device is

comparable to the lower pressure range of devices that use direct pressure actuation. The only constrain in attaining higher bending degrees in a shorter amount of time is the speed at which the vapor pressure of the fluid increases.

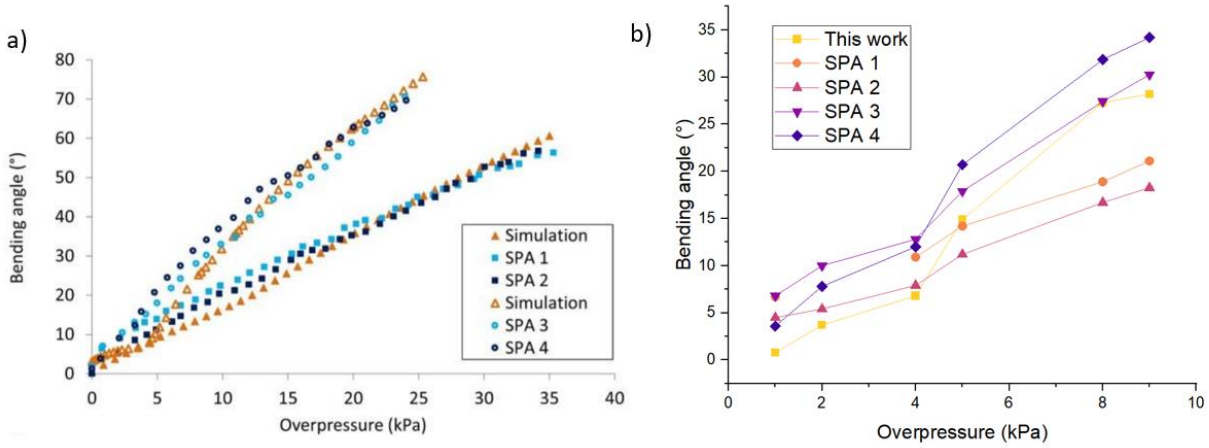

Figure 29. *a) Depiction of the bending angle of the different actuators tested and simulations by Terryn et al.*[38]*; b) Bending angle vs over pressure comparison between the literature results and the current work*

3.6. Pre-heating effect

Tests were conducted on the effect the use of the device soon after the termination of an actuation has on the bending angle. The test portrays its behavior over the time period of 320 s and can be depicted in *Figure 30.* As it can be observed, the device in pristine conditions reaches bending angles of around 20° in the first 120 s at 27 V and a composition of 5 g ethanol and 25 mg carbon black. When the voltage is turned off, the bending angle starts decreasing, reaching about half of its actuation in 120 s. When the voltage is passed through the device in the pre-heated conditions, the bending angle goes above 25° in 80 s. The time required to reach similar bending actuation is now half of the time the device takes in its pristine conditions. When comparing the pressure and temperature graphs, *Figure 31* and *32,* it can be observed that the starting point of the second actuation is 60 °C and a corresponding remaining pressure build-up of 3 kPa. Therefore, it can be drawn that the use of the actuator at short time intervals will result in faster actuation. This is in accordance with the observations drawn by Chellatoan et al. in regard to the behavior their designed actuator has when tested in its pristine vs. pre-heated conditions.[54]

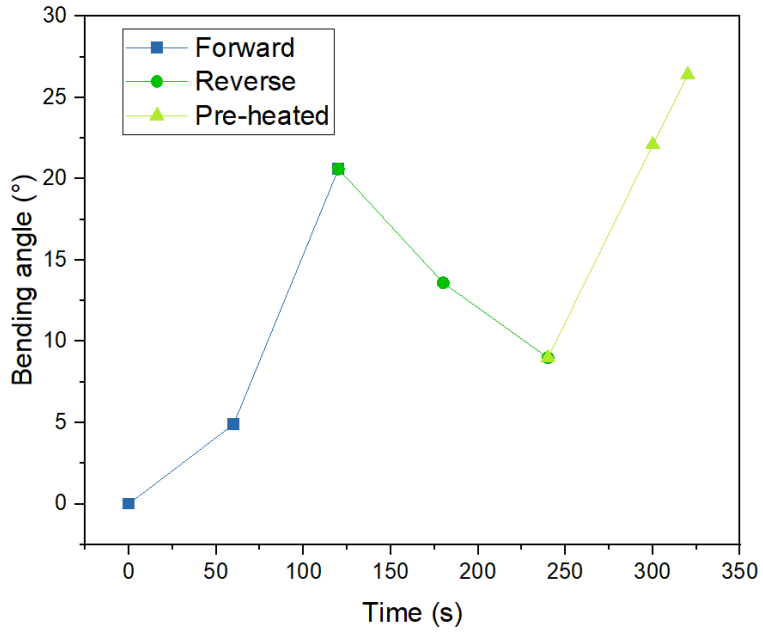

Figure 30. *Bending angle as a function of time for a cyclic actuation*

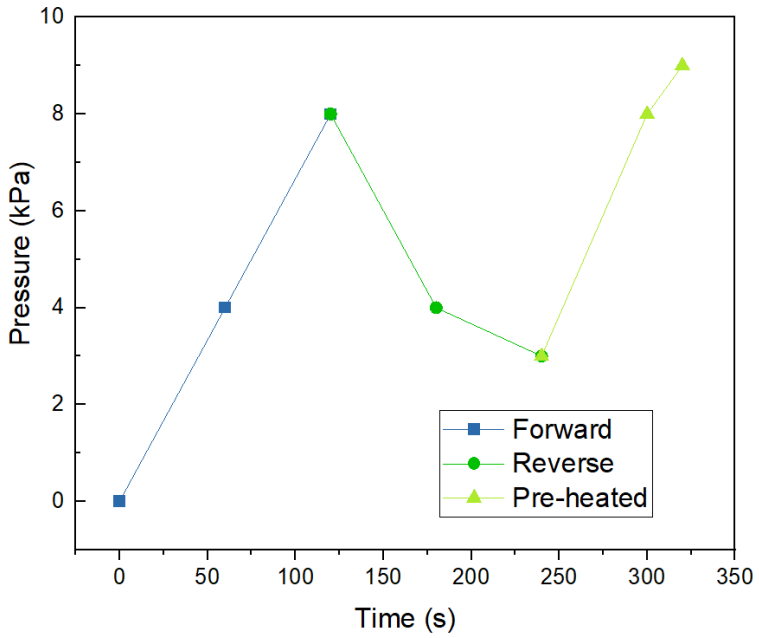

Figure 31. *Pressure build-up as a function of time for a cyclic actuation*

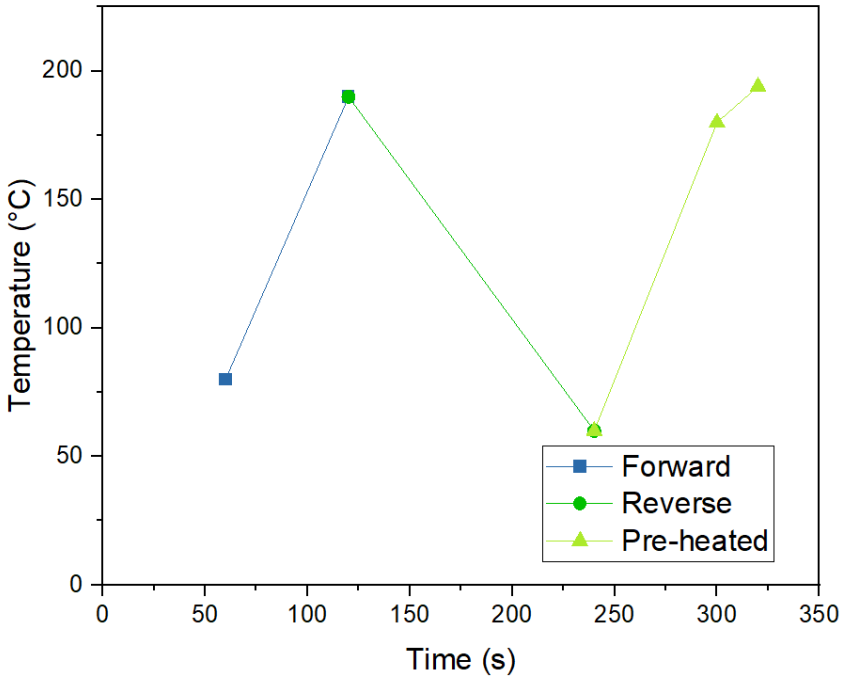

Figure 32. *Temperature profile as a function of time for a cyclic actuation*

3.7. Mechanical properties of the polyketone layer

The thermo-mechanical properties of the polyketone layer were characterized by means of rheology and the profile is shown in *Figure 33 a.* As it can be observed, the complex modulus G* decreases with the increase in temperature, as it is expected with the facilitation of the rDA reaction and the increase in the linear chain mobility of the polymer. Moreover, at temperatures above 60 °C, this approaches values close to zero, suggesting that both the storage and the loss moduli decrease significantly with temperature. Therefore, the polyketone layer turns from a more rigid into a rubbery material when heated up above 40 °C. This feature is essential in order to ensure that the actuation of the device is not constrained by the self-healing layer.

This 3:1 furan:maleimide formulation was chosen in order to promote faster softening of the material with the increase in temperature, and a lower rigidity at room temperature due to a lower crosslinking density. When comparing the complex modulus as a function of temperature of this polyketone with other formulations using –OH groups, plasticizers and Pk-Da with a lower furan:maleimide ratio (*See Figure 33 b*[101]*),* it can be observed that the formulation used in this work reaches the lowest complex modulus. The data presented show that the chosen formulation is the most suitable in terms of its flexibility for the studied application.

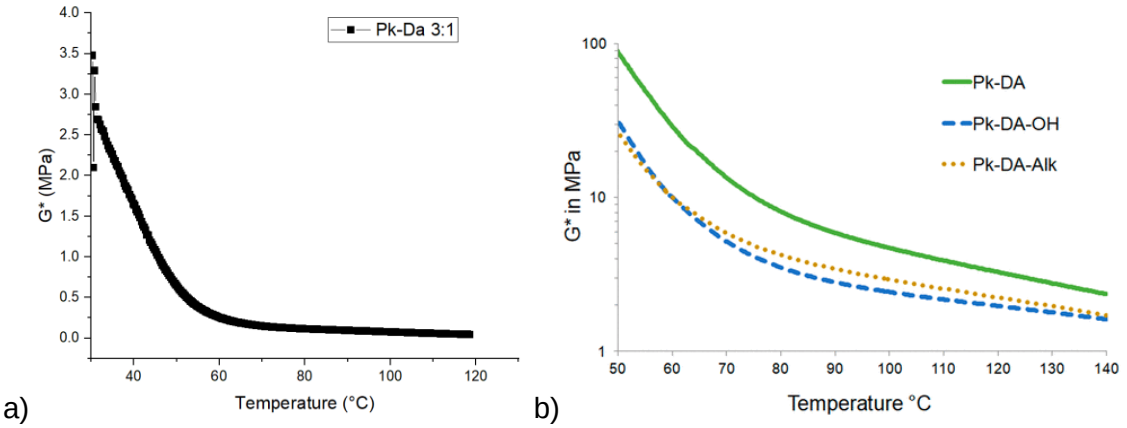

Figure 33. *a) The complex modulus as a function of temperature of the formulation used in: a) this work; b) other works with a lower Pk-DA ratio, a Pk functionalized with –OH groups and an alkyl-grafted polyketone (plasticizers)*[101]

The amplitude sweeps at different temperatures give additional information on the characteristics of the polymer. As presented in *Figure 34 a),* the storage (G') and the loss (G'') moduli undergo significant changes due to the partial breaking of the network when strain is applied. Since the material shows more rigid behavior at temperatures as low as 50 °C, this will break under lower strain. When investigating the behavior of the material at 110 °C (see *Figure 34 b)*, the value of the loss modulus is shown to be low, while the value of the storage modulus is relatively higher and does not show significant changes throughout the characterization. Low loss moduli mean that there is low energy dissipation to the environment with the applied strain. Therefore, the polyketone behaves almost entirely like an elastic material over the strain interval tested with no visible yield point. However, with the increase in strain, a decrease in the storage modulus and an increase in the loss modulus would be expected due to the partially broken network mobility being able to promote more viscous-like behavior.

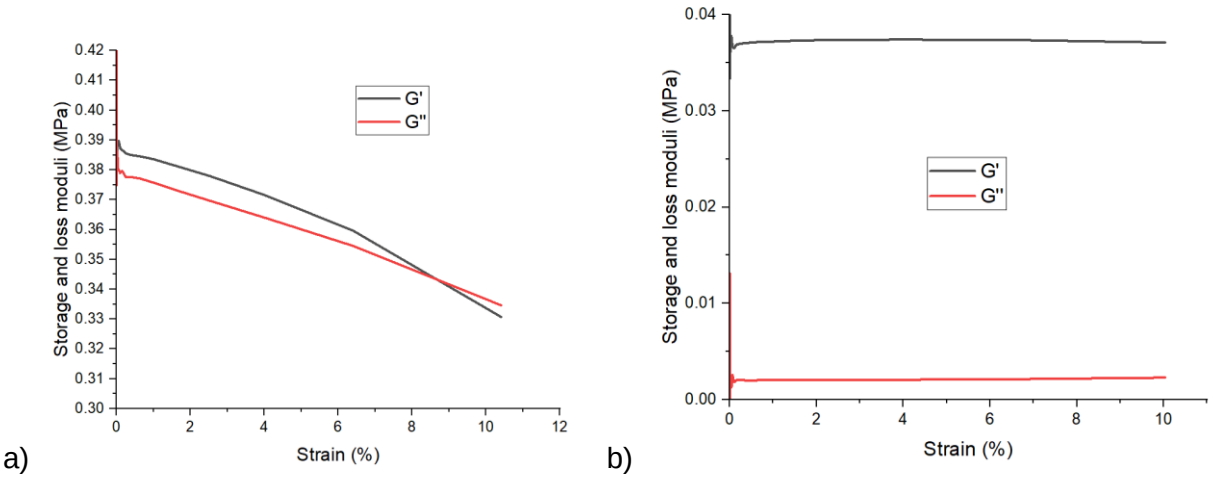

Figure 34. *Amplitude sweep of the polyketone layer at a) 50 °C; b) 110 °C*

3.8. Self-healing tests

Small cuts of different sizes were made into the self-healing polymer and the level of self-healing was recorded under the microscope before and after the actuation. Micro-damages were observed to have the capacity to self-heal almost entirely when electricity is passed through for the amount of time required for the device to exposed to 120 °C for 2 minutes, as it can be depicted in *Figure 35.* However, the size of the scratch poses limitations as, with the increase in its size, the healing ability decreases (see *Figure 36).*

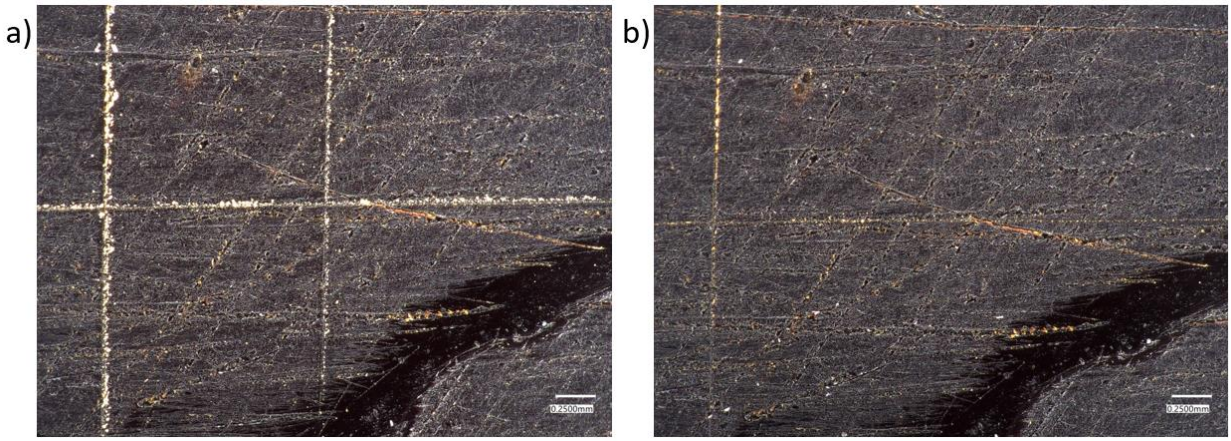

Figure 35. *a) Polyketone layer before healing with different sized scratches made on its surface (scale bar reads: 0.2500 mm); b) Polyketone layer after healing by means of actuation and exposure to high temperatures (scale bar reads: 0.2500 mm)*

While the material proves its self-healing capabilities in some of the carried-out experiments, other samples fail to show good healing behavior (see *Figure 36*). One of the reasons for this could be the difficulty in carving reproducible scratches onto the device due to the specific shape and rubbery nature of the samples. This prevents us from using a standard micro-scratching equipment that ensures good reproducibility of the scratch size. Therefore, manual scratches needed to be made with relatively decreased precision in terms of the width and depth. In this manner, it was observed that mainly scratches that were done very lightly could promote self-healing of the material with temperature application.

Another important phenomenon that deviates from the standard way of conducting self-healing tests is the mobility of the device during the temperature application. As temperature increases, the ethanol inside of the actuator starts to evaporate, resulting in the bending effect. The motion of the self-healing layer could potentially disrupt the healing process, similarly to the disruption of the healing process of a scratch on the skin surface of a finger when in motion.

While the low furan:maleimide ratio is expected to facilitate the self-healing ability of the polyketone layer in a short time[88], the results reveal that further improvements could be done in order to achieve higher levels of healability.

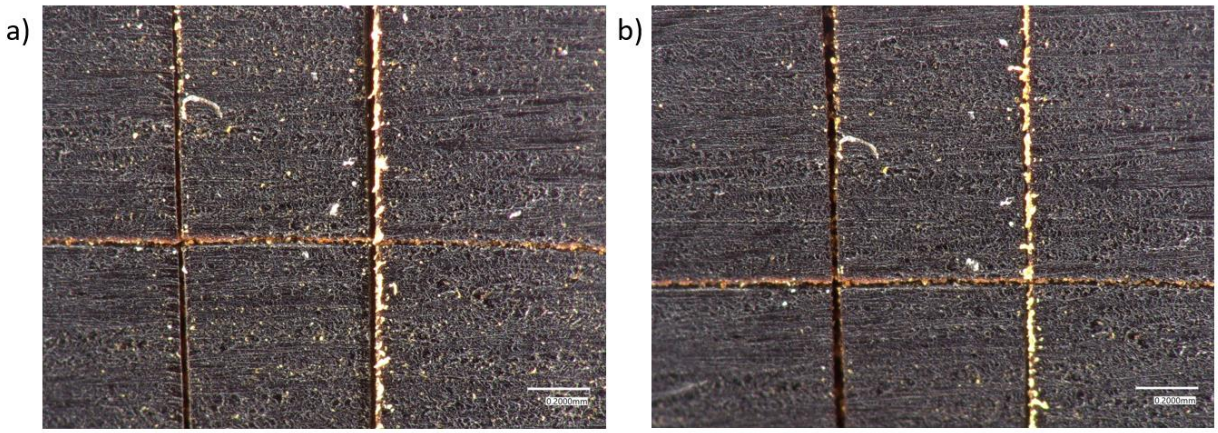

Figure 36. *a) Polyketone layer before healing with wide scratches made on its surface (scale bar reads: 0.2000 mm); b) Polyketone layer after exposure to high temperatures and significant oscillatory movement during actuation (scale bar reads: 0.2000 mm)*

Terryn et al. reported a Diels-Alder self-healing pneumatic robotic hand that could achieve complete self-healing of macroscopic cuts as thick as 0.39 mm and 8-9.5 mm long at temperatures as low as 80 °C kept constant for 40 minutes.[38] The recovery of the mechanical properties is reported to take approximately 24 hours. An autonomous Diels-Alder self-healing

soft robot was developed that could achieve self-healing at room temperature.[90] However, in order to be able to do that, its crosslinking density needed to be exceptionally low so that it would possess high flexibility. This comes with a negative impact on the mechanical properties, which could pose problems in terms of its force output during its application. 3D printed passive fingers with application in food manipulation were reported to achieve macroscopic self-healing at 90 °C for 30 minutes.[102] Although the device studied in this work can heal damages in a very short amount of time when compared to other works, the extent of healing could benefit from further improvements.

3.9. Performance limitations

Throughout the experimental work it was observed that by adjusting parameters such as the amount of ethanol, carbon black and voltage the bending angle of the actuator can be maximized to around 30° in less than 2 minutes. Nonetheless, the extent of bending showed clear limitations when compared to other studies. Direct pressure actuation can achieve close to full bending (over 70°) at pressures of 25 kPa almost instantaneously[38], while phase transition bending using ethanol and resistive microfiber of steel wool can achieve good bending in less than a minute with pressure build-ups inside of the device of up to 15 kPa.[54]

Further increase in the power input was shown to improve the actuation time, however the materials pose limitations in terms of the temperatures they can withstand. Orozco et al. report that a change in the mechanical properties of the self-healing polyketone can be observed upon exposure to temperatures as high as 150 °C, suggesting the possibility of side reactions taking place that would lead to an alteration of the mechanical properties with an effect on the self-healing properties.[103] This is undesirable; therefore, the power input was reduced once the device reached this value throughout the performed experiments. Temperature control was, however, difficult to achieve considering that at the higher tested power input values the temperature profile would increase rapidly exceeding the 150 °C limit. Additionally, considering that it takes about 10 minutes for the device to cool down to room temperature once the power is off, in a scenario where it would be used repeatedly with short time intervals in between each actuation, the starting temperature of the device after the first use would be higher than room temperature. This leads to faster actuation, since the boiling temperature would be reached over a shorter period of time than in pristine conditions. A direct consequence is fast over-heating, in which case voltage regulation is required.

The self-healing polymer poses limitations in regard to two different aspects: its insulating properties are limited; therefore, the gripping side of the actuator heats up to similar temperatures

reached inside of the device. Temperatures of around 100-150 °C on the outer surface of the actuator make it unfavorable to use in most applications. It was observed that when this would be immersed in a thin layer of Sylgard 184, the registered external temperatures would drop by a few tens of Celsius degrees, making the insulating properties of polyketones inferior when compared to silicone rubbers. Additionally, the current formulation showed limitations in its healing abilities, being able to heal only superficial scratches.

Lastly, the permeability of the silicone elastomer during actuation and the heat distribution are of fundamental concern. Although the reports presented in the *Methodology* chapter suggest that at higher temperatures the permeability of the material decreases, the opposite trend was observed throughout the experimental work. This could be explained by the fact that the material reached high temperatures locally (the area in direct contact with the wire), leaving the chambers of the device almost unaffected by the resistive heating. This has two consequences. Firstly, since pressure build-up is reported to increase the permeability of the silicone elastomer at temperatures close to room temperature (see *Figure 20*), the loss in ethanol during the actuation is observed to be higher than when the pressure inside the device is 0. This results in a significant loss after several actuations, which directly impacts the performance of the device. Additionally, since the actuation was carried out vertically, the ethanol was located on the bottom half of the device. When electricity was passed through the device, the chambers corresponding to the free end inflated preferentially, resulting in uneven actuation due to uneven heat distribution. Since the insertion of carbon black has a limited effect on the heat transfer enhancement, other approaches are worth considering for further investigations and are discussed in the next section.

4. Recommendations for future work

The design of the device could be further optimized in order to achieve faster actuation. One of the most relevant parameters is reported to be the inside wall thickness of the chambers facing one another. Decreasing the current thickness of the respective walls could result in improved actuation due to improved ease of swelling with pressure build-up. Additionally, by increasing the thickness of the bottom layer (especially the PDMS layer) or by using different materials with better insulating properties, the insulation of the gripping side could be improved.

A different resistor (design) could be used in order to ensure even heat distribution throughout the device, facilitating the heating of the chambers as well as the self-healing material. One such example would be the change in the placement or the design of the resistive wire. Miriyev et al. show that the use of a triple-coiled wire could decrease the heating time by 40%.[53] Using a resistive flexible material that fills up the chambers of the device, such as microfiber of steel wool

or a microfiber mat are reported to give good heat distribution and fast actuation.[54,99] This could also reduce the permeability of the material during actuation, resulting in less ethanol loss.

Different formulations of the self-healing material that provide better self-healing abilities and mechanical properties could replace the current one. Further reduction in the furan:maleimide ratio or functionalization with –OH groups are a few examples in that direction. Orozco et al. showed that by incorporating –OH groups into the backbone of the Diels-Alder polyketone, scratches of up to approximately 100 μm could be repaired. Additionally, the stiffness of the polymer is reduced with this formulation, which is a desired feature for the current application, since a brittle material at room temperature would pose a higher risk of breakage during handling. Although the flexibility of the formulation used in this work is greater than the one using –OH groups, the self-healing ability shows an overall lower performance. This could, however, be attributed to the different conditions in which the self-healing experiments were tested (see *Section 3.8).*

Lastly, choosing a lower boiling point liquid that shows stability at room temperature and is safe in case of leakage is worth considering. Chellatoan et al. report that the actuation time could be reduced by choosing a solvent with a lower total boiling point.[54] When they compare the performance of ethanol versus acetone, the latter shows faster actuation and unbending when electricity is turned off. However, acetone leakage is a safety concern, while its stability at room temperature is questionable.

5. Conclusion

In the recent years, soft robotic actuators have been shown to have great potential over rigid, metallic ones, due to their compliance with the surrounding environment and the ability to interact safely with humans and fragile objects. The downside to those materials is their susceptibility to damages due to their soft and flexible properties, which causes self-healing soft robots to gain more attention. In this work, we investigated several possible designs that could be adopted in order to make a self-healing soft robotic gripper, namely shape memory polymers, bilayer actuators and pneumatic actuators. A few properties were considered, including the scalability to macroscopic dimensions suitable for industrial applications and the ability to achieve repeated actuation using the same stimulus required to induce the self-healing effect. The final design consisted of an electroactive self-healing gripper capable of actuation under low voltage. Although the design was similar to pneumatic grippers, unlike those, the bending was induced by a different stimulus than direct pressure. The actuation was achieved by phase transition of ethanol at elevated temperatures and the heat transfer was produced by electricity passed through a

resistive coiled wire. The self-healing material used was a thermoresversible Diels-Alder polyketone with low crosslinking density that can self-heal within the same temperature range required to induce actuation. With this design, bending motion could be achieved in less than 1 minute at powers lower than 30 W and superficial scars with widths lower than 30 μm could be healed in less than 3 minutes during actuation at elevated temperatures. Additionally, it was demonstrated that by increasing the amount of ethanol, the extent of actuation could be improved, while the speed of actuation decreased due to a decrease in the heat transfer. Carbon black was used in combination with ethanol in order to improve the heat transfer, however this approach only showed limited enhancement. Increasing the voltage resulted in faster actuation, as well as using the device in its pre-heated state, yet there is a need for voltage control due to the temperature limitations the materials possess. This work stands as proof of concept for the development of a soft robotic gripper that can self-heal during actuation. With this approach, there is no need to terminate the actuation and apply an external stimulus to heal damages induced while in use, reducing the reparation time significantly. This is an important characteristic and constitutes the novelty of this work, considering that most injuries take place during actuation. With further optimization of the heat transfer, heat insulation of the material, actuation speed and the extent of healing, this design shows great potential in the field of soft robotics.

6. Bibliography

(1) Walker, J.; Zidek, T.; Harbel, C.; Yoon, S.; Strickland, F. S.; Kumar, S.; Shin, M. Soft Robotics: A Review of Recent Developments of Pneumatic Soft Actuators. *Actuators* **2020**, *9* (1). https://doi.org/10.3390/act9010003.

(2) Whitesides, G. M. Soft Robotics. *Angewandte Chemie - International Edition*. Wiley-VCH Verlag April 9, 2018, pp 4258–4273. https://doi.org/10.1002/anie.201800907.

(3) Terryn, S.; Langenbach, J.; Roels, E.; Brancart, J.; Bakkali-Hassani, C.; Poutrel, Q. A.; Georgopoulou, A.; George Thuruthel, T.; Safaei, A.; Ferrentino, P.; Sebastian, T.; Norvez, S.; Iida, F.; Bosman, A. W.; Tournilhac, F.; Clemens, F.; van Assche, G.; Vanderborght, B. A Review on Self-Healing Polymers for Soft Robotics. *Materials Today*. Elsevier B.V. July 1, 2021, pp 187–205. https://doi.org/10.1016/j.mattod.2021.01.009.

(4) Ewoldt, R. H. Extremely Soft: Design with Rheologically Complex Fluids. *Soft Robotics*. Mary Ann Liebert Inc. March 1, 2014, pp 12–20. https://doi.org/10.1089/soro.2013.1508.

(5) Hughes, J.; Culha, U.; Giardina, F.; Guenther, F.; Rosendo, A.; Iida, F. Soft Manipulators and Grippers: A Review. *Frontiers Robotics AI*. Frontiers Media S.A. November 1, 2016. https://doi.org/10.3389/frobt.2016.00069.

(6) Mosadegh, B.; Polygerinos, P.; Keplinger, C.; Wennstedt, S.; Shepherd, R. F.; Gupta, U.; Shim, J.; Bertoldi, K.; Walsh, C. J.; Whitesides, G. M. Pneumatic Networks for Soft

Robotics That Actuate Rapidly. *Advanced Functional Materials* **2014**, *24* (15), 2163–2170. https://doi.org/10.1002/adfm.201303288.

(7) Nassar, J. M.; Rojas, J. P.; Hussain, A. M.; Hussain, M. M. From Stretchable to Reconfigurable Inorganic Electronics. *Extreme Mechanics Letters*. Elsevier Ltd December 1, 2016, pp 245–268. https://doi.org/10.1016/j.eml.2016.04.011.

(8) Coyle, S.; Majidi, C.; LeDuc, P.; Hsia, K. J. Bio-Inspired Soft Robotics: Material Selection, Actuation, and Design. *Extreme Mechanics Letters*. Elsevier Ltd July 1, 2018, pp 51–59. https://doi.org/10.1016/j.eml.2018.05.003.

(9) Majidi, C. Soft Robotics: A Perspective - Current Trends and Prospects for the Future. *Soft Robotics*. Mary Ann Liebert Inc. March 1, 2014, pp 5–11. https://doi.org/10.1089/soro.2013.0001.

(10) Case, J. C.; White, E. L.; Kramer, R. K. Soft Material Characterization for Robotic Applications. *Soft Robotics* **2015**, *2* (2), 80–87. https://doi.org/10.1089/soro.2015.0002.

(11) O'Halloran, A.; O'Malley, F.; McHugh, P. A Review on Dielectric Elastomer Actuators, Technology, Applications, and Challenges. *Journal of Applied Physics* **2008**, *104* (7). https://doi.org/10.1063/1.2981642.

(12) Tolley, M. T.; Shepherd, R. F.; Mosadegh, B.; Galloway, K. C.; Wehner, M.; Karpelson, M.; Wood, R. J.; Whitesides, G. M. A Resilient, Untethered Soft Robot. *Soft Robotics* **2014**, *1* (3), 213–223. https://doi.org/10.1089/soro.2014.0008.

(13) Sun, J. Y.; Zhao, X.; Illeperuma, W. R. K.; Chaudhuri, O.; Oh, K. H.; Mooney, D. J.; Vlassak, J. J.; Suo, Z. Highly Stretchable and Tough Hydrogels. *Nature* **2012**, *489* (7414), 133–136. https://doi.org/10.1038/nature11409.

(14) Hager, M. D.; Bode, S.; Weber, C.; Schubert, U. S. Shape Memory Polymers: Past, Present and Future Developments. *Progress in Polymer Science*. Elsevier Ltd October 1, 2015, pp 3–33. https://doi.org/10.1016/j.progpolymsci.2015.04.002.

(15) Meng, H.; Li, G. A Review of Stimuli-Responsive Shape Memory Polymer Composites. *Polymer*. Elsevier Ltd April 19, 2013, pp 2199–2221. https://doi.org/10.1016/j.polymer.2013.02.023.

(16) Behl, M.; Lendlein, A. Triple-Shape Polymers. *Journal of Materials Chemistry* **2010**, *20* (17), 3335–3345. https://doi.org/10.1039/b922992b.

(17) Hu, J.; Zhu, Y.; Huang, H.; Lu, J. Recent Advances in Shape-Memory Polymers: Structure, Mechanism, Functionality, Modeling and Applications. *Progress in Polymer Science*. December 2012, pp 1720–1763. https://doi.org/10.1016/j.progpolymsci.2012.06.001.

(18) Julich-Gruner, K. K.; Löwenberg, C.; Neffe, A. T.; Behl, M.; Lendlein, A. Recent Trends in the Chemistry of Shape-Memory Polymers. *Macromolecular Chemistry and Physics* **2013**, *214* (5), 527–536. https://doi.org/10.1002/macp.201200607.

(19) Yang, Y.; Chen, Y.; Wei, Y.; Li, Y. 3D Printing of Shape Memory Polymer for Functional Part Fabrication. *International Journal of Advanced Manufacturing Technology* **2016**, *84* (9–12), 2079–2095. https://doi.org/10.1007/s00170-015-7843-2.

(20) Fan, J.; Li, G. High Performance and Tunable Artificial Muscle Based on Two-Way Shape Memory Polymer. *RSC Advances* **2017**, *7* (2), 1127–1136. https://doi.org/10.1039/c6ra25024f.

(21) Bodaghi, M.; Damanpack, A. R.; Liao, W. H. Triple Shape Memory Polymers by 4D Printing. *Smart Materials and Structures* **2018**, *27* (6). https://doi.org/10.1088/1361-665X/aabc2a.
(22) Ionov, L. Polymeric Actuators. *Langmuir* **2015**, *31* (18), 5015–5024. https://doi.org/10.1021/la503407z.
(23) Montero De Espinosa, L.; Meesorn, W.; Moatsou, D.; Weder, C. Bioinspired Polymer Systems with Stimuli-Responsive Mechanical Properties. *Chemical Reviews*. American Chemical Society October 25, 2017, pp 12851–12892. https://doi.org/10.1021/acs.chemrev.7b00168.
(24) Apsite, I.; Stoychev, G.; Zhang, W.; Jehnichen, D.; Xie, J.; Ionov, L. Porous Stimuli-Responsive Self-Folding Electrospun Mats for 4D Biofabrication. *Biomacromolecules* **2017**, *18* (10), 3178–3184. https://doi.org/10.1021/acs.biomac.7b00829.
(25) Behl, M.; Kratz, K.; Zotzmann, J.; Nöchel, U.; Lendlein, A. Reversible Bidirectional Shape-Memory Polymers. *Advanced Materials* **2013**, *25* (32), 4466–4469. https://doi.org/10.1002/adma.201300880.
(26) Pilz da Cunha, M.; Foelen, Y.; Engels, T. A. P.; Papamichou, K.; Hagenbeek, M.; Debije, M. G.; Schenning, A. P. H. J. On Untethered, Dual Magneto- and Photoresponsive Liquid Crystal Bilayer Actuators Showing Bending and Rotating Motion. *Advanced Optical Materials* **2019**, *7* (7). https://doi.org/10.1002/adom.201801604.
(27) Jiang, Z. C.; Xiao, Y. Y.; Tong, X.; Zhao, Y. Selective Decrosslinking in Liquid Crystal Polymer Actuators for Optical Reconfiguration of Origami and Light-Fueled Locomotion. *Angewandte Chemie - International Edition* **2019**, *58* (16), 5332–5337. https://doi.org/10.1002/anie.201900470.
(28) Guo, M.; Wu, Y.; Xue, S.; Xia, Y.; Yang, X.; Dzenis, Y.; Li, Z.; Lei, W.; Smith, A. T.; Sun, L. A Highly Stretchable, Ultra-Tough, Remarkably Tolerant, and Robust Self-Healing Glycerol-Hydrogel for a Dual-Responsive Soft Actuator. *Journal of Materials Chemistry A* **2019**, *7* (45), 25969–25977. https://doi.org/10.1039/c9ta10183g.
(29) Jiang, Z.; Tan, M. L.; Taheri, M.; Yan, Q.; Tsuzuki, T.; Gardiner, M. G.; Diggle, B.; Connal, L. A. Strong, Self-Healable, and Recyclable Visible-Light-Responsive Hydrogel Actuators. *Angewandte Chemie* **2020**, *132* (18), 7115–7122. https://doi.org/10.1002/ange.201916058.
(30) Hu, Y.; Xu, A.; Liu, J.; Yang, L.; Chang, L.; Huang, M.; Gu, W.; Wu, G.; Lu, P.; Chen, W.; Wu, Y. Multifunctional Soft Actuators Based on Anisotropic Paper/Polymer Bilayer Toward Bioinspired Applications. *Advanced Materials Technologies* **2019**, *4* (3). https://doi.org/10.1002/admt.201800674.
(31) Hu, Y.; Liu, J.; Chang, L.; Yang, L.; Xu, A.; Qi, K.; Lu, P.; Wu, G.; Chen, W.; Wu, Y. Electrically and Sunlight-Driven Actuator with Versatile Biomimetic Motions Based on Rolled Carbon Nanotube Bilayer Composite. *Advanced Functional Materials* **2017**, *27* (44). https://doi.org/10.1002/adfm.201704388.
(32) Wang, W.; Xiang, C.; Zhu, Q.; Zhong, W.; Li, M.; Yan, K.; Wang, D. Multistimulus Responsive Actuator with GO and Carbon Nanotube/PDMS Bilayer Structure for Flexible and Smart Devices. *ACS Applied Materials and Interfaces* **2018**, *10* (32), 27215–27223. https://doi.org/10.1021/acsami.8b08554.

(33) Song, J.; Zhang, Y. From Two-Dimensional to Three-Dimensional Structures: A Superior Thermal-Driven Actuator with Switchable Deformation Behavior. *Chemical Engineering Journal* **2019**, *360*, 680–685. https://doi.org/10.1016/j.cej.2018.12.026.
(34) El-Atab, N.; Mishra, R. B.; Al-Modaf, F.; Joharji, L.; Alsharif, A. A.; Alamoudi, H.; Diaz, M.; Qaiser, N.; Hussain, M. M. Soft Actuators for Soft Robotic Applications: A Review. *Advanced Intelligent Systems* **2020**, *2* (10), 2000128. https://doi.org/10.1002/aisy.202000128.
(35) Ionov, L. Soft Microorigami: Self-Folding Polymer Films. *Soft Matter* **2011**, *7*(15), 6786-6791.
(36) Kang, D. J.; An, S.; Yarin, A. L.; Anand, S. Programmable Soft Robotics Based on Nano-Textured Thermo-Responsive Actuators. *Nanoscale* **2019**, *11* (4), 2065–2070. https://doi.org/10.1039/c8nr08215d.
(37) Ilievski, F.; Mazzeo, A. D.; Shepherd, R. F.; Chen, X.; Whitesides, G. M. Soft Robotics for Chemists. *Angewandte Chemie* **2011**, *123* (8), 1930–1935. https://doi.org/10.1002/ange.201006464.
(38) Terryn, S.; Brancart, J.; Lefeber, D.; Assche, G. van; Vanderborght, B. *Self-Healing Soft Pneumatic Robots*; 2017; Vol. 2.
(39) Martinez, R. v.; Fish, C. R.; Chen, X.; Whitesides, G. M. Elastomeric Origami: Programmable Paper-Elastomer Composites as Pneumatic Actuators. *Advanced Functional Materials* **2012**, *22* (7), 1376–1384. https://doi.org/10.1002/adfm.201102978.
(40) Pelrine, R.; Kornbluh, R.; Pei, Q.; Stanford, S.; Oh, S.; Eckerle, J.; Full, R.; Rosenthal, M.; Meijer, K. *Dielectric Elastomer Artificial Muscle Actuators: Toward Biomimetic Motion*; 2002.
(41) Kwon, G. H.; Park, J. Y.; Kim, J. Y.; Frisk, M. L.; Beebe, D. J.; Lee, S. H. Biomimetic Soft Multifunctional Miniature Aquabots. *Small* **2008**, *4* (12), 2148–2153. https://doi.org/10.1002/smll.200800315.
(42) Jager, E. W. H.; Inganäs, O.; Lundström, I. *Microrobots for Micrometer-Size Objects in Aqueous Media: Potential Tools for Single-Cell*; 2000; Vol. 288.
(43) Shintake, J.; Rosset, S.; Schubert, B.; Floreano, D.; Shea, H. Versatile Soft Grippers with Intrinsic Electroadhesion Based on Multifunctional Polymer Actuators. *Advanced Materials* **2016**, *28* (2), 231–238. https://doi.org/10.1002/adma.201504264.
(44) Pelrine, R.; Kornbluh, R.; Pei, Q.; Joseph, J. *High-Speed Electrically Actuated Elastomers with Strain Greater Than 100%*; 2000; Vol. 287.
(45) Niklaus, M.; Rosset, S.; Dubois, P.; Shea, H. Ion-Implanted Compliant Electrodes Used in Dielectric Electroactive Polymer Actuators with Large Displacement. In *Procedia Chemistry*; 2009; Vol. 1, pp 702–705. https://doi.org/10.1016/j.proche.2009.07.175.
(46) Acome, E.; Mitchell, S. K.; Morrissey, T. G.; Emmett, M. B.; Benjamin, C.; King, M.; Radakovitz, M.; Keplinger, C. *Hydraulically Amplified Self-Healing Electrostatic Actuators with Muscle-like Performance*.
(47) Ji, X.; Liu, X.; Cacucciolo, V.; Imboden, M.; Civet, Y.; Haitami, A. el; Cantin, S.; Perriard, Y.; Shea, H. *An Autonomous Untethered Fast Soft Robotic Insect Driven by Low-Voltage Dielectric Elastomer Actuators*; 2019.

(48) Sohn, J.-W.; Choi, S.-B. Various Robots Made from Piezoelectric Materials and Electroactive Polymers: A Review. *International Journal of Mechanical Systems Engineering* **2017**, *3* (1). https://doi.org/10.15344/2455-7412/2017/122.
(49) Zhao, Q.; Liu, S.; Chen, J.; He, G.; Di, J.; Zhao, L.; Su, T.; Zhang, M.; Hou, Z. Fast-Moving Piezoelectric Micro-Robotic Fish with Double Caudal Fins. *Robotics and Autonomous Systems* **2021**, *140*. https://doi.org/10.1016/j.robot.2021.103733.
(50) Behl, M.; Razzaq, M. Y.; Lendlein, A. Multifunctional Shape-Memory Polymers. *Advanced Materials*. August 17, 2010, pp 3388–3410. https://doi.org/10.1002/adma.200904447.
(51) Shintake, J.; Cacucciolo, V.; Shea, H.; Floreano, D. Soft Biomimetic Fish Robot Made of Dielectric Elastomer Actuators. *Soft Robotics* **2018**, *5* (4), 466–474. https://doi.org/10.1089/soro.2017.0062.
(52) Hu, W.; Lum, G. Z.; Mastrangeli, M.; Sitti, M. Small-Scale Soft-Bodied Robot with Multimodal Locomotion. *Nature* **2018**, *554* (7690), 81–85. https://doi.org/10.1038/nature25443.
(53) Miriyev, A.; Stack, K.; Lipson, H. Soft Material for Soft Actuators. *Nature Communications* **2017**, *8* (1). https://doi.org/10.1038/s41467-017-00685-3.
(54) Chellattoan, R.; Yudhanto, A.; Lubineau, G. Low-Voltage-Driven Large-Amplitude Soft Actuators Based on Phase Transition. *Soft Robotics* **2020**, *7* (6), 688–699. https://doi.org/10.1089/soro.2019.0150.
(55) Lei, M.; Chen, Z.; Lu, H.; Yu, K. Recent Progress in Shape Memory Polymer Composites: Methods, Properties, Applications and Prospects. *Nanotechnology Reviews*. De Gruyter January 1, 2019, pp 327–351. https://doi.org/10.1515/ntrev-2019-0031.
(56) Yakacki, C. M.; Shandas, R.; Lanning, C.; Rech, B.; Eckstein, A.; Gall, K. Unconstrained Recovery Characterization of Shape-Memory Polymer Networks for Cardiovascular Applications. *Biomaterials* **2007**, *28* (14), 2255–2263. https://doi.org/10.1016/j.biomaterials.2007.01.030.
(57) Hearon, K.; Wierzbicki, M. A.; Nash, L. D.; Landsman, T. L.; Laramy, C.; Lonnecker, A. T.; Gibbons, M. C.; Ur, S.; Cardinal, K. O.; Wilson, T. S.; Wooley, K. L.; Maitland, D. J. A Processable Shape Memory Polymer System for Biomedical Applications. *Advanced Healthcare Materials* **2015**, *4* (9), 1386–1398. https://doi.org/10.1002/adhm.201500156.
(58) Behl, M.; Lendlein, A. *Shape-Memory Polymers*; 2007.
(59) Amend, J.; Cheng, N.; Fakhouri, S.; Culley, B. Soft Robotics Commercialization: Jamming Grippers from Research to Product. *Soft Robotics* **2016**, *3* (4), 213–222. https://doi.org/10.1089/soro.2016.0021.
(60) Kingsley, D. A.; Quinn, R. D. *Fatigue Life and Frequency Response of Braided Pneumatic Actuators*; 2002.
(61) Miron, G.; Plante, J. S. Design Principles for Improved Fatigue Life of High-Strain Pneumatic Artificial Muscles. *Soft Robotics* **2016**, *3* (4), 177–185. https://doi.org/10.1089/soro.2016.0011.
(62) Govorčin Bajsić, E.; Rek, V.; Agić, A. Thermal Degradation of Polyurethane Elastomers: Determination of Kinetic Parameters. *Journal of Elastomers and Plastics* **2003**, *35* (4), 311–323. https://doi.org/10.1177/009524403034393.
(63) Fischer, H. R.; Semprimoschnig, C.; Mooney, C.; Rohr, T.; van Eck, E. R. H.; Verkuijlen, M. H. W. Degradation Mechanism of Silicone Glues under UV Irradiation and Options for

Designing Materials with Increased Stability. *Polymer Degradation and Stability* **2013**, *98* (3), 720–726. https://doi.org/10.1016/j.polymdegradstab.2012.12.022.

(64) Billiet, S.; Hillewaere, X. K. D.; Teixeira, R. F. A.; du Prez, F. E. Chemistry of Crosslinking Processes for Self-Healing Polymers. *Macromolecular Rapid Communications*. February 25, 2013, pp 290–309. https://doi.org/10.1002/marc.201200689.

(65) Toohey, K. S.; Sottos, N. R.; Lewis, J. A.; Moore, J. S.; White, S. R. Self-Healing Materials with Microvascular Networks. *Nature Materials* **2007**, *6* (8), 581–585. https://doi.org/10.1038/nmat1934.

(66) Kötteritzsch, J.; Stumpf, S.; Hoeppener, S.; Vitz, J.; Hager, M. D.; Schubert, U. S. One-Component Intrinsic Self-Healing Coatings Based on Reversible Crosslinking by Diels-Alder Cycloadditions. *Macromolecular Chemistry and Physics* **2013**, *214* (14), 1636–1649. https://doi.org/10.1002/macp.201200712.

(67) Cordier, P.; Tournilhac, F.; Soulié-Ziakovic, C.; Leibler, L. Self-Healing and Thermoreversible Rubber from Supramolecular Assembly. *Nature* **2008**, *451* (7181), 977–980. https://doi.org/10.1038/nature06669.

(68) Bose, R. K.; Hohlbein, N.; Garcia, S. J.; Schmidt, A. M.; van der Zwaag, S. Connecting Supramolecular Bond Lifetime and Network Mobility for Scratch Healing in Poly(Butyl Acrylate) Ionomers Containing Sodium, Zinc and Cobalt. *Physical Chemistry Chemical Physics* **2015***, 17*(3), 1697-1704. https://doi.org/10.1039/c0xx00000x.

(69) Jin, H.; Mangun, C. L.; Stradley, D. S.; Moore, J. S.; Sottos, N. R.; White, S. R. Self-Healing Thermoset Using Encapsulated Epoxy-Amine Healing Chemistry. *Polymer* **2012**, *53* (2), 581–587. https://doi.org/10.1016/j.polymer.2011.12.005.

(70) White, S. R.; Sottos, N. R.; Geubelle, P. H.; Moore, J. S.; Kessler, M. R.; Sriram, S. R.; Brown, E. N.; Viswanathan, S. Autonomic Healing of Polymer Composites. *Nature*. February 15, 2001, pp 794–797. https://doi.org/10.1038/35057232.

(71) Bejan, A.; Lorente, S.; Wang, K. M. Networks of Channels for Self-Healing Composite Materials. *Journal of Applied Physics* **2006**, *100* (3). https://doi.org/10.1063/1.2218768.

(72) Torre-Muruzabal, A.; Daelemans, L.; van Assche, G.; de Clerck, K.; Rahier, H. Creation of a Nanovascular Network by Electrospun Sacrificial Nanofibers for Self-Healing Applications and Its Effect on the Flexural Properties of the Bulk Material. *Polymer Testing* **2016**, *54*, 78–83. https://doi.org/10.1016/j.polymertesting.2016.06.026.

(73) Ling, J.; Rong, M. Z.; Zhang, M. Q. Photo-Stimulated Self-Healing Polyurethane Containing Dihydroxyl Coumarin Derivatives. *Polymer* **2012**, *53* (13), 2691–2698. https://doi.org/10.1016/j.polymer.2012.04.016.

(74) van Damme, J.; van den Berg, O.; Brancart, J.; van Assche, G.; du Prez, F. A Novel Donor-π-Acceptor Anthracene Monomer: Towards Faster and Milder Reversible Dimerization. *Tetrahedron* **2019**, *75* (7), 912–920. https://doi.org/10.1016/j.tet.2019.01.007.

(75) Chen, Y.; Tang, Z.; Zhang, X.; Liu, Y.; Wu, S.; Guo, B. Covalently Cross-Linked Elastomers with Self-Healing and Malleable Abilities Enabled by Boronic Ester Bonds. *ACS Applied Materials and Interfaces* **2018**, *10* (28), 24224–24231. https://doi.org/10.1021/acsami.8b09863.

(76) Cao, L.; Fan, J.; Huang, J.; Chen, Y. A Robust and Stretchable Cross-Linked Rubber Network with Recyclable and Self-Healable Capabilities Based on Dynamic Covalent

Bonds. *Journal of Materials Chemistry A* **2019**, *7* (9), 4922–4933. https://doi.org/10.1039/c8ta11587g.

(77) Cui, J.; Campo, A. del. Multivalent H-Bonds for Self-Healing Hydrogels. *Chemical Communications* **2012**, *48* (74), 9302–9304. https://doi.org/10.1039/c2cc34701f.

(78) Burattini, S.; Colquhoun, H. M.; Fox, J. D.; Friedmann, D.; Greenland, B. W.; Harris, P. J. F.; Hayes, W.; MacKay, M. E.; Rowan, S. J. A Self-Repairing, Supramolecular Polymer System: Healability as a Consequence of Donor-Acceptor π-π Stacking Interactions. *Chemical Communications* **2009**, No. 44, 6717–6719. https://doi.org/10.1039/b910648k.

(79) Xu, C.; Nie, J.; Wu, W.; Fu, L.; Lin, B. Design of Self-Healable Supramolecular Hybrid Network Based on Carboxylated Styrene Butadiene Rubber and Nano-Chitosan. *Carbohydrate Polymers* **2019**, *205*, 410–419. https://doi.org/10.1016/j.carbpol.2018.10.080.

(80) Shi, Y.; Wang, M.; Ma, C.; Wang, Y.; Li, X.; Yu, G. A Conductive Self-Healing Hybrid Gel Enabled by Metal-Ligand Supramolecule and Nanostructured Conductive Polymer. *Nano Letters* **2015**, *15* (9), 6276–6281. https://doi.org/10.1021/acs.nanolett.5b03069.

(81) Sommazzi, A.; GARBASSI Enichem SpA, F. *OLEFIN-CARBON MONOXIDE COPOLYMERS*; 1997; Vol. 22.

(82) *United States Patent (19)*.

(83) Zhang, Y. *Chemical Modifications and Applications of Alternating Aliphatic Polyketones*.

(84) Khaghaninejad, S.; Heravi, M. M. Paal-Knorr Reaction in the Synthesis of Heterocyclic Compounds. In *Advances in Heterocyclic Chemistry*; Academic Press Inc., 2014; Vol. 111, pp 95–146. https://doi.org/10.1016/B978-0-12-420160-6.00003-3.

(85) Murphy, E. B.; Wudl, F. The World of Smart Healable Materials. *Progress in Polymer Science (Oxford)*. January 2010, pp 223–251. https://doi.org/10.1016/j.progpolymsci.2009.10.006.

(86) Yuliati, F.; Hong, J.; Indriadi, K. S.; Picchioni, F.; Bose, R. K. Thermally Reversible Polymeric Networks from Vegetable Oils. *Polymers* **2020**, *12* (8). https://doi.org/10.3390/POLYM12081708.

(87) Gandini, A. The Furan/Maleimide Diels-Alder Reaction: A Versatile Click-Unclick Tool in Macromolecular Synthesis. *Progress in Polymer Science*. January 2013, pp 1–29. https://doi.org/10.1016/j.progpolymsci.2012.04.002.

(88) Orozco, F.; Li, J.; Ezekiel, U.; Niyazov, Z.; Floyd, L.; Lima, G. M. R.; Winkelman, J. G. M.; Moreno-Villoslada, I.; Picchioni, F.; Bose, R. K. Diels-Alder-Based Thermo-Reversibly Crosslinked Polymers: Interplay of Crosslinking Density, Network Mobility, Kinetics and Stereoisomerism. *European Polymer Journal* **2020**, *135*. https://doi.org/10.1016/j.eurpolymj.2020.109882.

(89) Shepherd, R. F.; Stokes, A. A.; Nunes, R. M. D.; Whitesides, G. M. Soft Machines That Are Resistant to Puncture and That Self Seal. *Advanced Materials* **2013**, *25* (46), 6709–6713. https://doi.org/10.1002/adma.201303175.

(90) Terryn, S.; Brancart, J.; Roels, E.; van Assche, G.; Vanderborght, B. Room Temperature Self-Healing in Soft Pneumatic Robotics: Autonomous Self-Healing in a Diels-Alder Polymer Network. *IEEE Robotics and Automation Magazine* **2020**, *27* (4), 44–55. https://doi.org/10.1109/MRA.2020.3024275.

(91) Zhang, Y.; Yin, X. Y.; Zheng, M.; Moorlag, C.; Yang, J.; Wang, Z. L. 3D Printing of Thermoreversible Polyurethanes with Targeted Shape Memory and Precise in Situ Self-Healing Properties. *Journal of Materials Chemistry A* **2019**, *7* (12), 6972–6984. https://doi.org/10.1039/c8ta12428k.
(92) Martinez, R. v.; Branch, J. L.; Fish, C. R.; Jin, L.; Shepherd, R. F.; Nunes, R. M. D.; Suo, Z.; Whitesides, G. M. Robotic Tentacles with Three-Dimensional Mobility Based on Flexible Elastomers. *Advanced Materials* **2013**, *25* (2), 205–212. https://doi.org/10.1002/adma.201203002.
(93) Vaicekauskaite, J.; Mazurek, P.; Vudayagiri, S.; Ladegaard Skov, A. Silicone Elastomer Map: Design the Ideal Elastomer; SPIE-Intl Soc Optical Eng, 2019; p 61. https://doi.org/10.1117/12.2515305.
(94) Seghir, R.; Arscott, S. Extended PDMS Stiffness Range for Flexible Systems. *Sensors and Actuators, A: Physical* **2015**, *230*, 33–39. https://doi.org/10.1016/j.sna.2015.04.011.
(95) Zhang, Y.; Broekhuis, A. A.; Picchioni, F. Thermally Self-Healing Polymeric Materials: The next Step to Recycling Thermoset Polymers? *Macromolecules* **2009**, *42* (6), 1906–1912. https://doi.org/10.1021/ma8027672.
(96) Blume, I.; Schwering, P. J. F.; Mulder, M. H. v; Smolders, C. A. *Vapour Sorption and Permeation Properties of Poly (Dimethylsiloxane) Films**.
(97) Leemann, M.; Eigenberger, G.; Strathmann, H. *Vapour Permeation for the Recovery of Organic Solvents from Waste Air Streams: Separation Capacities and Process Optimization*; 1996; Vol. 113.
(98) Harmston, Don. *Materials Challenge Diversification and the Future*; Society for the Advancement of Material and Process Engineering, 1995.
(99) Kang, D. J.; An, S.; Yarin, A. L.; Anand, S. Programmable Soft Robotics Based on Nano-Textured Thermo-Responsive Actuators. *Nanoscale* **2019**, *11* (4), 2065–2070. https://doi.org/10.1039/c8nr08215d.
(100) Li, X.; Duan, H.; Lv, P.; Yi, X. Soft Actuators Based on Liquid-Vapor Phase Change Composites. *Soft Robotics* **2021**, *8* (3), 251–261. https://doi.org/10.1089/soro.2020.0018.
(101) Orozco, F.; Kaveh, M.; Santosa, D. S.; Lima, G. M. R.; Gomes, D. R.; Pei, Y.; Araya-Hermosilla, R.; Moreno-Villoslada, I.; Picchioni, F.; Bose, R. K. Electroactive Self-Healing Shape Memory Polymer Composites Based on Diels–Alder Chemistry. *ACS Applied Polymer Materials* **2021**, acsapm.1c00999. https://doi.org/10.1021/acsapm.1c00999.
(102) Roels, E.; Terryn, S.; Brancart, J.; Verhelle, R.; van Assche, G.; Vanderborght, B. Additive Manufacturing for Self-Healing Soft Robots. *Soft Robotics* **2020**, *7* (6), 711–723. https://doi.org/10.1089/soro.2019.0081.
(103) Orozco, F.; Niyazov, Z.; Garnier, T.; Migliore, N.; Zdvizhkov, A. T.; Raffa, P.; Moreno-Villoslada, I.; Picchioni, F.; Bose, R. K. Maleimide Self-Reaction in Furan/Maleimide-Based Reversibly Crosslinked Polyketones: Processing Limitation or Potential Advantage? *Molecules* **2021**, *26* (8). https://doi.org/10.3390/molecules26082230.
(104) Atif, R.; Inam, F. Reasons and Remedies for the Agglomeration of Multilayered Graphene and Carbon Nanotubes in Polymers. *Beilstein Journal of Nanotechnology* **2016**, *7* (1), 1174–1196. https://doi.org/10.3762/bjnano.7.109.
(105) Riesco, R.; Boyer, L.; Blosse, S.; Lefebvre, P. M.; Assemat, P.; Leichle, T.; Accardo, A.; Malaquin, L. Water-in-PDMS Emulsion Templating of Highly Interconnected Porous

Architectures for 3D Cell Culture. *ACS Applied Materials and Interfaces* **2019**, *11* (32), 28631–28640. https://doi.org/10.1021/acsami.9b07564.
(106) Miriyev, A.; Trujillo, C.; Caires, G.; Lipson, H. Rejuvenation of Soft Material-Actuator. *MRS Communications* **2018**, *8* (2), 556–561. https://doi.org/10.1557/mrc.2018.30.
(107) Institute of Electrical and Electronics Engineers. *2018 IEEE International Conference on Soft Robotics (RoboSoft) : 24-28 April 2018.*

7. Appendix

Figure 1. *Device manufacturing attempt using a straight stainless-steel wire*

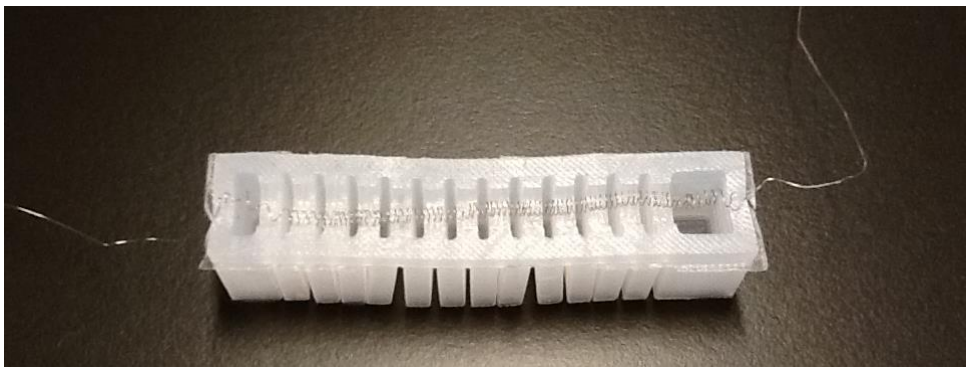

Figure 2. *Final device manufacturing using a 60 cm long coiled stainless-steel wire*

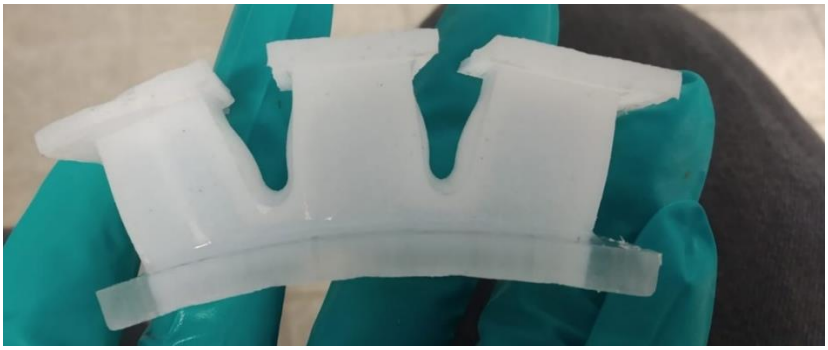

Figure 3. *Initial actuator design with 3 chambers and a large gap between each chamber*

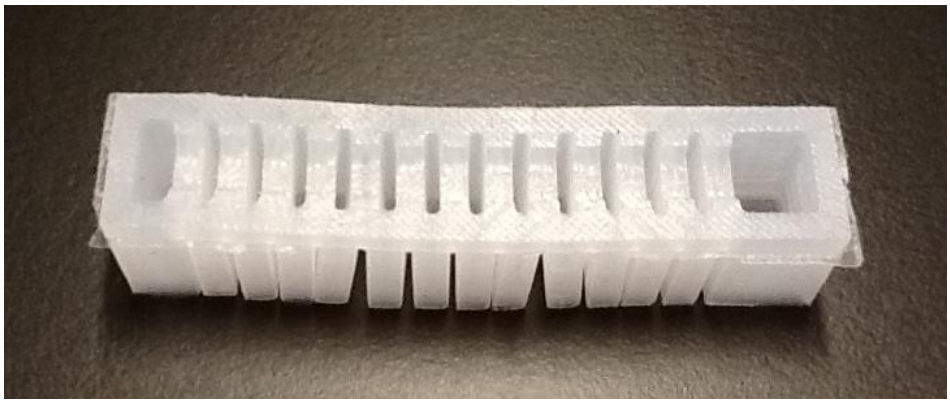

Figure 4. *Hollow device before closing made out of Ecoflex 00-50*

Figure 5. *Device enclosed by cellulosic paper and Sylgard 184 PDMS*

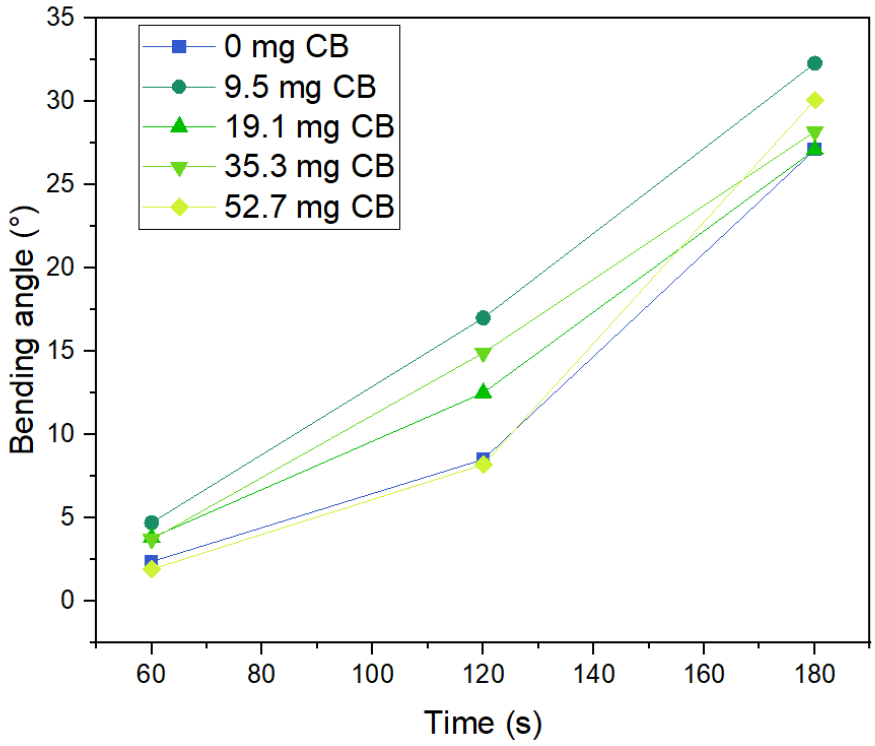

Figure 6. *Bending angle vs time at different tested amounts of carbon black and 4.5 g ethanol*

Figure 6 depicts different amounts of carbon black tested on their effect on the bending angle over time. Similarly to the trend observed in *Figure 26,* the highest impact on the bending angle can be observed around 120 s. The presumption that with the increase in the amount of carbon black there would be an increase in the bending angle over time is only true for some of the tested values. While the odd trend for the 9.5 mg carbon black could be assigned to a slightly higher voltage applied throughout the experiment in comparison to the other points, the 52.7 mg carbon black odd trend can only be related to the heat capacity of the material. There is a limit to which the bending angle is enhanced by the increase of added carbon black, considering that with the increase in volume of carbon black, there is a need for more energy in order to heat up the contents of the device (similarly to the trend observed for the increase in mass of ethanol depicted in *Figures 24 and 25).* This graph shows that at values higher than 50 mg carbon black the efficiency in heating the total increased volume up is decreased and overpowers the heat conductive abilities that would be expected to enhance the speed of heat distribution.

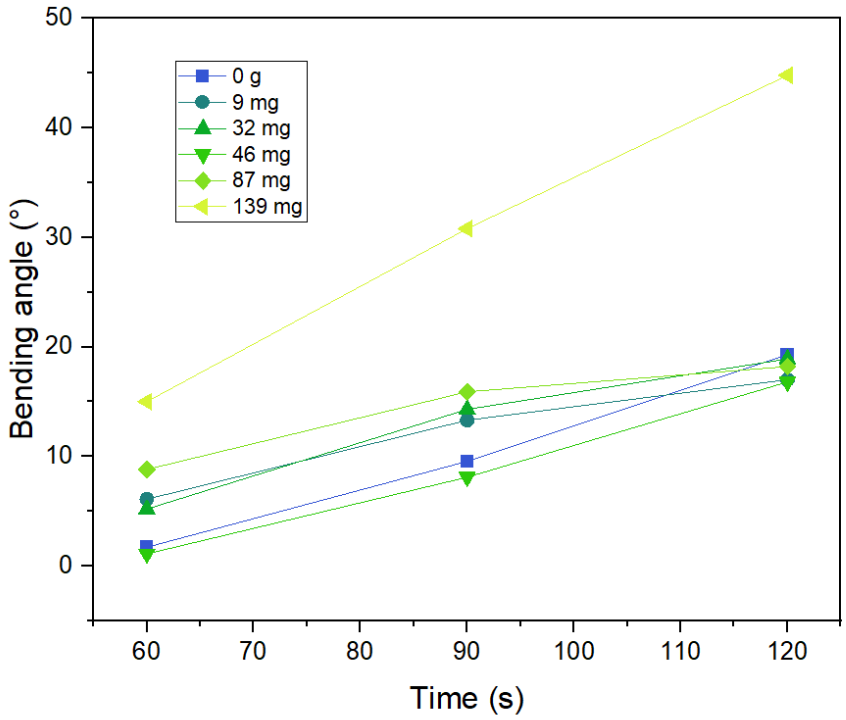

Figure 7. *Bending angle vs time at different tested amounts of carbon black and 4-4.2 g ethanol*

Figure 7 portrays the carbon black experiments carried out on a different device, at a lower amount of ethanol. The highest registered bending angle for 139 mg added carbon black can be explained by the over-pressurized device at this composition, such that at room temperature its walls were slightly expanded. This signifies that the starting pressure is higher than 0, which enhances the device abilities to reach higher pressures than the rest in a shorter amount of time. Overall, all the other tested compositions showed higher bending angle at 60 and 120 s, with the exception of the one with 46 mg carbon black. The mass of ethanol for this trial was about 0.2 g lower than most of the other compositions. The discrepancy in the results could be attributed to the slight variation in the mass of ethanol throughout the experimental work, which could have an effect on the total pressure build-up over time and the actuation angle. As it can be noticed, the heating efficiency is affected differently than in the tests carried out at 4.5 g ethanol (*Figure A5)*. Due to a lower amount of ethanol, this device can withhold a higher mass of carbon black before its performance is affected.

Other experimental attempts:

Various attempts were carried out in order to achieve the final design. At first, an electroactive three-layer actuator composed of Sylgard 184 PDMS, multi-walled carbon

nanotubes (MWCNs) and polyketone was studied. The working principle of the device was inspired by the volume change of other reported bilayer actuators described in the *Introduction* chapter. The MWCN layer would enhance the resistive heat, the PDMS layer would expand preferentially and the device would bend towards the self-healing polyketone side. The first major challenge during this approach was the formation of the MWCN layer. Due to the well-documented Van der Waals forces, they tend to agglomerate and, as a result, the layer formation on different substrates (glass, Teflon, filter paper) fail, as depicted in *Figure A8.*[104] A few ways to tackle those are by using organic solvents and dispersion methods and functionalization. The first two proposed solutions were investigated by using different organic solvents (chloroform, dimethylformamide) and by using various centrifugation mixing times. Treatment with nitric acid was also investigated, however none of the attempted solutions improved the agglomeration problem.

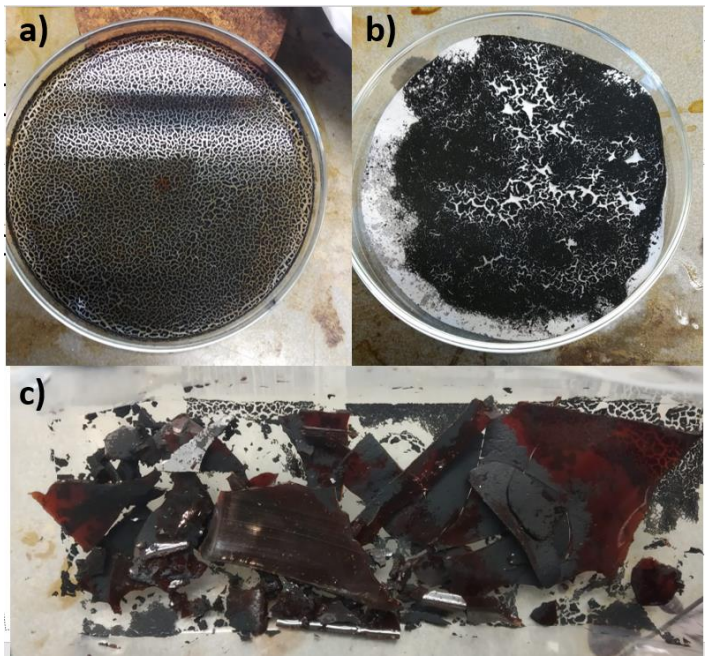

Figure 8. *Depiction of the MCWN layer on a) glass substrate; b) filter paper; c) Teflon boat over a polyketone layer*

A bilayer actuator consisting of only PDMS and polyketone was attempted using the spin coating technique (*see Figure 9)*. Difficulties emerged from the removal of the micro-meter range layers from the coating substrate. Macroscopic bilayers were attempted with no visible actuation upon heat application (*see Figure 10)*. Subsequently it was discovered that the volume expansion of Sylgard 184 PDMS was approximately the same as the polyketone, therefore no preferential

volume expansion could emerge. In order to tackle this problem, air pores were induced inside of the PDMS material by a technique described by Riesco et al., however this did not improve its thermal expansion coefficient.[105]

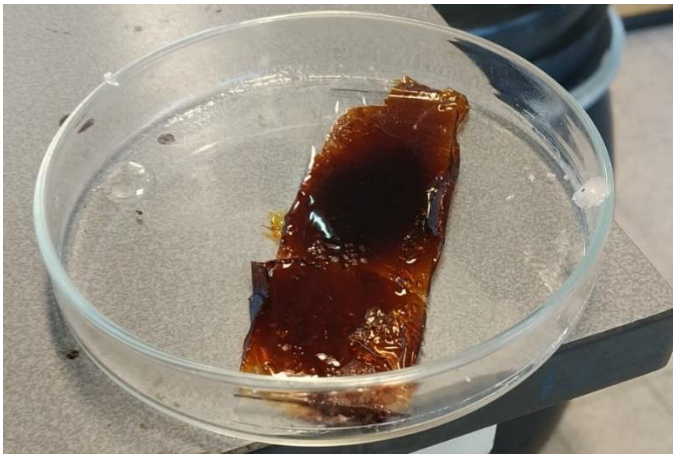

Figure 10. *Spin coated bilayer composed of polyketone on the bottom and Sylgard 184 PDMS on top glued over a glass substrate*

New multi-layer actuator attempts were performed using Ecoflex (00-30 and 00-50) with ethanol droplets dispersed through its matrix as one layer, paper as a binding layer and polyketone for the third layer. A resistive wire passed through the device would result in the Joule heating effect. The working principle of the actuator is based on the preferential volumetric expansion of the Ecoflex layer when the ethanol inside of this reaches its boiling point.[53] Ecoflex showed excellent volume expansion abilities, however ethanol evaporation from the Ecoflex matrix would impact the actuator performance within hours. By the time the polyketone layer would cure together with the Ecoflex + paper layer, there would be hardly any actuation due to almost complete ethanol evaporation. Therefore, the full design with working capabilities was never achieved, however the excellent bending of Ecoflex + paper soon after the curing process can be shown in *Figure 11.*

***Figure 11**. Ecoflex + ethanol and paper actuator fully bent during heat application*

Since the last design was the closest to a functional device, further literature study was carried out on the topic and a few suggestions could be added for future work. Although rejuvenation of the actuator once all ethanol evaporated was studied to show good results, this process is impractical for the studied application.[106] Ethanol evaporation can be tackled by encapsulating the device in 'skin' that would not allow it to diffuse through. One proposed example for such a material was Teflon.[53] Another challenge that comes with this design is the rapid failure of the device due to local over-heating in the area the resistive wire passes through. Bilodeanu et al. developed a similar silicone-based actuator where the resistive wire was replaced by a silicone-based conductive composite, which was shown to have better compatibility with the device and comparable performance.[107] The overall heat distribution is improved, resulting in a longer life-time of the actuator. Therefore, with all the improvements suggested from literature, further work could be carried out on this design in order to achieve a self-healing bilayer actuator.